Research Square

Preprints are preliminary reports that have not undergone peer review.
They should not be considered conclusive, used to inform clinical practice,
or referenced by the media as validated information.

Integrated analysis of laser-captured glomerular proteome characterizes the expression and functional role of APOE in membranous nephropathy

CHANG LU

351939278@qq.com

The 924th Hospital of Joint Logistic Support Force of PLA

Donge Tang

ShenZhen People's Hospital

Guang Hu

The 924th Hospital of Joint Logistic Support Force of PLA

Hualin Ma

ShenZhen People's Hospital

Guimian Zou

The 924th Hospital of Joint Logistic Support Force of PLA

Shenping Xie

The 924th Hospital of Joint Logistic Support Force of PLA

Jingjing Dong

ShenZhen People's Hospital

Zhifeng Luo

The 924th Hospital of Joint Logistic Support Force of PLA

Yaoshuang Zou

The 924th Hospital of Joint Logistic Support Force of PLA

Yong Dai

Anhui University of Science and Technology

Huaizhou Chen

The 924th Hospital of Joint Logistic Support Force of PLA

Jingsheng Ma

The 924th Hospital of Joint Logistic Support Force of PLA

Research Article

Keywords: membranous nephropathy, glomerular proteomics, APOE, multi-omics, machine learning, biomarker, molecular targeted therapy

Posted Date: November 19th, 2026

DOI: https://doi.org/10.21203/rs.3.rs-11227389/v1

License: This work is licensed under a Creative Commons Attribution 4.0 International License. Read Full License

Additional Declarations: No competing interests reported.

Abstract

Background

MN is a prevalent primary glomerular disease causing adult nephrotic syndrome. Clinically, invasive renal biopsy acts as the pathological gold standard, while the widely used serological anti-PLA2R antibody has limited sensitivity and cannot reflect glomerular lesion severity. Conventional immunosuppressive regimens face frequent drug resistance and relapse, and core tissue-derived pathogenic regulators remain poorly defined. This study aimed to to identify reliable MN biomarkers and clarify underlying mechanisms,providing new approaches for precise diagnosis and treatment

Methods

Glomeruli from 5 MN patients and 8 normal controls were isolated via LCM and detected by LC-MRM-MS proteomics. We integrated GO/KEGG enrichment, PPI network, WGCNA, three machine learning algorithms to screen hub proteins. IHC and WB were used to verify candidate protein expression. Public single-cell dataset GSE241302 was applied for in silico knockdown simulation, and AutoDock Vina performed molecular docking to screen targeted small-molecule compounds.

Results

We identified 29 glomerular DEPs (18 upregulated, 11 downregulated) enriched in complement-coagulation, lipid metabolism, oxidative stress and ECM remodeling. PPI and WGCNA revealed APOE, FBLN1 and HP as core hub proteins. Three machine learning algorithms converged on HPT, FBLN1 and APOE as diagnostic markers with AUC>0.95. IHC and WB confirmed markedly higher glomerular APOE in MN ($p = 0.0035$, $p < 0.0001$). In silico APOE knockdown restored glutathione metabolism, detoxification, lipid signaling and tubular SLC transporters to relieve podocyte damage and proteinuria. Eight high-affinity APOE-targeted BRD compounds were screened via molecular docking, with BRD-K76617868 and BRD-K93023739 showing the best binding capacity.

Conclusion

APOE acts as a high-performance glomerular diagnostic biomarker and central pathogenic hub of MN, which mediates renal damage via crosstalk of lipid metabolism, immune inflammation, redox imbalance and tubular dysfunction. This research provides novel theoretical basis for non-invasive auxiliary diagnosis and molecular targeted therapy of MN

Background

Membranous nephropathy (MN) is one of the predominant primary glomerular diseases leading to adult nephrotic syndrome, featured by subepithelial immune complex deposition, glomerular basement membrane thickening, refractory proteinuria, and progressive renal fibrosis; a considerable proportion of untreated patients eventually advance to end-stage renal disease (ESRD), imposing heavy clinical and socioeconomic burdens worldwide[1, 2],therapeutic management of MN still face prominent unmet clinical demands, despite substantial advances in disease pathogenesis and treatment research in recent years[3, 4].

Renal biopsy remains the gold standard for definitive pathological diagnosis of MN per the KDIGO 2021 glomerular disease guideline[5], yet it carries inherent risks of bleeding, infection and renal injury, and is unsuitable for patients with severe coagulation dysfunction or advanced renal insufficiency. Circulating anti-PLA2R antibody, the most widely used serological biomarker at present, shows robust diagnostic specificity but insufficient sensitivity, failing to identify PLA2R-negative MN subtypes and lacking capacity to quantitatively reflect glomerular lesion severity and dynamic pathological remodeling within renal tissues[6, 7]. Beyond PLA2R and THSD7A, novel podocyte antigens including NELL-1 and EXT1 have been continuously uncovered, but single antigen detection cannot fully recapitulate the complex multi-pathway pathological cascades of MN.Therefore, high-performance, tissue-derived protein biomarkers capable of reflecting glomerular pathological changes are urgently required to supplement existing serological indicators and facilitate non-invasive auxiliary diagnosis of MN.

In terms of treatment, the 2021 KDIGO guideline stratifies MN patients and recommends RAAS inhibitors for low-risk cases and immunosuppressants for moderate-to-high-risk individuals[8]. Although landmark trials MENTOR[9]and RI-CYCLO[10]confirm the remission effect of rituximab and cyclophosphamide, 20%–30% of patients suffer drug resistance or relapse after immunosuppression[11, 12]. Long-term generalized immunosuppression also increases risks of severe infection and secondary tumors. Existing therapies mainly deplete B cells globally, without targeted drugs acting on glomerular pathogenic pathways. Emerging research identifies lipid dysregulation as a key driver of MN podocyte injury and sclerosis, but core lipid regulatory molecules bridging systemic metabolism and renal lesions lack systematic multi-omics and clinical tissue validation[13, 14].

Global hotspots of contemporary MN research mainly cover three dimensions: identification of novel diagnostic biomarkers, dissection of multi-layered pathogenic mechanisms, and development of targeted therapeutic molecules. First, multi-omics technology represented by glomerular proteomics, single-cell transcriptomics and weighted gene co-expression network analysis (WGCNA) has become a mainstream strategy to screen differential molecular signatures and clarify cell-type-specific pathogenic pathways[15, 16]. Second, machine learning algorithms including LASSO regression, random forest and RFE-SVM are widely applied to filter stable diagnostic panels from high-dimensional omics data, greatly improving the efficiency and accuracy of biomarker screening, and providing a technical basis for the construction of quantitative diagnostic models with high AUC values[17, 18]. Third, based on hub pathogenic molecules excavated from omics datasets, molecular docking virtual screening of small-

molecule compounds is emerging as a key preclinical approach to explore targeted therapeutic drugs, laying a theoretical foundation for developing low-toxicity, precise intervention agents for MN[19, 20].

Updated systematic reviews and clinical trials published in 2023–2026 have systematically summarized the latest progress of MN diagnosis, pathogenesis and therapeutic management, covering population-based cohort risk factor analysis, differential comparison of immunosuppressive regimens[21], tumor risk evaluation in PLA2R-associated MN, and gene-environment interaction research in idiopathic MN cohorts[22, 23].Nevertheless, most existing omics studies of MN merely perform preliminary bioinformatic mining, and no effective and reliable tissue-specific biomarkers have yet been identified through comprehensive multi-dimensional experimental validation.

To address the above clinical bottlenecks and research gaps, Our study combined glomerular proteomics, bioinformatic mining, machine learning screening and co-expression network analysis to mine consensus hub protein candidate biomarkers closely correlated with MN lesions. After multi-level clinical specimen validation and cellular mechanistic exploration, we further predicted potential targeted small-molecule compounds for this core molecule. Collectively, this work aims to identify reliable glomerular biomarkers for MN, reveal its pathogenic mechanisms, and provide novel theoretical basis and translational reference for precision diagnosis and molecular targeted therapy of membranous nephropathy.

Methods

1.Data Collection and Preprocessing

Data from our previous research of Jingjing Dong,the protein Expressing of glomeruli in membranous nephropathy by method of laser capture microdissection(LCM) and mass spectrometry（MS）was used to conduct the proteomic analysis,renal tissues form

5 MN patients by renal puncture and 8 healthy tissues from kidney transplant donors were recruited as normal controls(NC)[24].Kidney tissue was harvested and processed for routine formalin-fixed paraffin-embedded (FFPE) renal biopsy sectioning to generate histological glass slides. Middle panel: Glomeruli were precisely isolated from paraffin sections using the Leica LMD7000 laser microdissection system; dissected glomerular samples were collected and preserved at − 80°C for subsequent omics analysis. All participants provided written informed consent before sample collection.This project was approved by the Shenzhen People’s Hospital and the First Affiliated Hospital of Jinan University.(approval number: LL-KY-2020167 KY-2020-034). This study adopted a standardized experimental workflow for renal tissue protein quantification using LC-MRM-MS. Tissues were homogenized in liquid nitrogen and lysed, followed by TCA-acetone protein precipitation, DTT reduction and iodoacetamide cysteine blocking. Purified proteins were quantified by Bradford, stored at − 80°C, and digested overnight with trypsin. Peptides spiked with β-galactosidase were separated by nano-LC and detected with MRM-MS. Totally 43584 peptides and 3708 proteins were quantitated.

Based on our published proteomic data from Dong et al, we adopted 3,708 unique proteins for differential expression analysis rather than the 43,584 unique peptides used in their original research.Data of proteins were processed via Skyline and analyzed in MSstats; proteins with Q < 0.05 and fold change(FC) > 1.2 were considered differentially expressed.The process above were showed in the workflow of Figure.1

2.Bioinformatic Analysis

All proteomic data analyses and visualization were performed in R(v4.2.1). Differential protein expression(DEP) was calculated via limma; DEPs were screened with thresholds $|\log_2 FC| \geq 1$ and $P < 0.05$, visualized as volcano plots using ggplot2. Z-score normalized DEP abundance matrices underwent unsupervised hierarchical clustering (Euclidean distance, complete linkage) with pheatmap for heatmap display. Gene Ontology (GO) and Kyoto Encyclopedia of Genes and Genomes(KEGG) enrichment analyses were implemented by clusterProfiler via hypergeometric tests ($P < 0.05$). Top enriched GO terms (BP/CC/MF) were plotted as bar charts, while KEGG enrichment results were presented as bubble plots in ggplot2, where bubble color mapped to $-\log_{10}$(P-value) and size represented enriched DEPs count. Eight normal control and five membranous nephropathy samples were compared throughout all analyses.

3.WGCNA (Weighted Gene Co-expression Network Analysis)

Weighted gene co-expression network analysis(WGCNA) was implemented in R (v4.2.1) with the WGCNA package. A proper soft threshold power was screened by evaluating scale-free topology model fit R^2 and mean connectivity to construct scale-free co-expression network. Adjacency matrix was transformed into topological overlap matrix, followed by hierarchical clustering and dynamic tree cutting to partition proteins into distinct co-expression modules. Module eigengene values were calculated to compute Pearson correlations between each module and clinical traits. Gene significance and module membership of all proteins were quantified for key modules. Hub proteins within critical modules were identified. GO and KEGG functional enrichment for module proteins were performed via clusterProfiler (hypergeometric test, $P < 0.05$). All visualization outputs were generated using the ggplot2 package.

4.Protein-protein Interaction(PPI) and Hub protein Network

All analyses were performed in R (v4.2.1). Protein-protein interaction (PPI) network was constructed based on DEPs, topological parameters of each node were calculated to screen hub proteins via the igraph package. Nodes were ranked by degree centrality to identify core hub proteins and reconstruct the simplified hub protein interaction subnetwork. The ggforce and ggplot2 packages were used for network visualization. The networkD3 and ggplot2 packages jointly generated Sankey diagram to map the regulatory links from hub proteins to functional modules and membranous nephropathy pathological phenotypes. GO and KEGG enrichment results from prior analyses were integrated to annotate the functional classification of each hub protein.

5. Machine Learning Approaches

All machine learning algorithms and visualizations were implemented in R (v4.2.1). The glmnet package was used to perform LASSO logistic regression; cross-validated binomial deviance was calculated to determine optimal λ for variable screening, with regression coefficients output for feature filtering. RF modeling was conducted via the randomForest package, variable importance was quantified by mean decrease in accuracy and mean decrease Gini index. RFE-SVM feature selection was realized with the e1071 and caret packages. Intersected candidate markers from three algorithms were identified via Venn analysis. Receiver operating characteristic (ROC) curves with 95% confidence intervals were plotted using pROC to evaluate diagnostic performance of hub proteins. All graphical outputs were generated with the ggplot2 package.

6.Immunohistochemistry (IHC) and Western Blot (WB) Validation

Immunohistochemistry

Paraffin-embedded renal tissue sections from normal control and membranous nephropathy subjects underwent xylene dewaxing and gradient ethanol rehydration. Antigen retrieval was achieved via microwave heating in pH 6.0 citrate buffer. Endogenous peroxidase activity was blocked with 3% H_2O_2, and 1% BSA was used to block non-specific binding. Sections were incubated with primary antibodies against hub DEPs overnight at 4°C, followed by HRP-conjugated secondary antibody incubation at room temperature for 1 h. DAB chromogen developed positive staining, and hematoxylin counterstained cell nuclei. After dehydration and mounting, tissue images were captured under bright-field microscopy. The H-score system was applied for quantitative evaluation: staining intensity (0 = negative, 1 = weak, 2 = moderate, 3 = strong) multiplied by the percentage of positive stained cells (0–100%), yielding a final score ranging from 0 to 300 for intergroup expression comparison.

Western Blot

Total protein was extracted from renal cortex tissues using RIPA lysis buffer supplemented with protease and phosphatase inhibitor cocktail. Protein concentration was quantified by BCA assay, and equal protein aliquots were denatured at 95°C. Samples were separated by SDS-PAGE and wet-transferred to PVDF membranes. Membranes were blocked with 5% skim milk for 90 min, incubated with target primary antibodies at 4°C overnight, then HRP secondary antibodies for 1 h at room temperature. Protein bands were visualized with ECL chemiluminescence reagent. ImageJ software quantified band gray values, with GAPDH as internal reference to calculate relative protein expression. All quantitative data were analyzed via unpaired Student's t-test using GraphPad Prism 9; $P < 0.05$ indicated statistically significant differences.

7.Single-cell RNA-seq Data Mining and In Silico Key Protein Gene Knockdown Simulation

All single-cell transcriptomic computational analyses were executed using R software (v4.2.1). Raw single-cell RNA sequencing datasets were acquired from the public Gene Expression Omnibus database under accession number GSE241302[25]. Standard single-cell preprocessing workflows including quality control filtering, log-normalization, feature selection, PCA dimensional reduction, UMAP visualization, unsupervised Louvain clustering and cell subtype annotation were all completed relying on the Seurat package. Dot plots displaying canonical cell-type marker gene expression profiles and bar charts reflecting proportional shifts of cell populations between disease and control groups were generated with the ggplot2 package.In silico knockdown simulation targeting the gene encoding the screened key protein was performed to simulate transcriptional perturbation. Z-score transformation and statistical testing were conducted to identify downstream differentially expressed genes, with adjusted P-value < 0.05 set as the screening threshold. The igraph package was utilized to build protein-protein interaction networks of post-knockdown differential genes and extract core hub genes within the network. Functional enrichment of GO and KEGG pathways was performed via the clusterProfiler package with hypergeometric distribution tests ($P < 0.05$). Bubble plots and horizontal bar plots for enrichment results were visualized uniformly using ggplot2.

8.Small Molecule Virtual Screening and Molecular Docking Analysis

All computational modeling analyses were completed via Python and R (v4.2.1). The 3D structure of key target protein was downloaded from RCSB PDB and preprocessed with AutoDockTools, including water elimination, hydrogen supplementation and charge assignment. Small molecules from BRD compound library underwent virtual screening to calculate logit scores and binding probability; candidate compounds with high binding potential were screened by threshold, and screening distribution scatter plot was drawn by ggplot2.

Top hit compounds were subjected to molecular docking via AutoDock Vina. Binding pocket grid was defined for flexible ligand docking, and optimal binding conformations were retained. PyMOL was used to visualize protein-ligand 3D binding modes, annotate interacting amino acid residues and display hydrogen bond/hydrophobic interactions. All quantitative screening visualization was implemented in R.

Result

Proteomics Analysis of LCM-Isolated Glomeruli from MN and NC Samples

Firstly we used the data from our previous research of Jingjing Dong,which 5 MN and 8NC were included.The detailed clinical baseline information of normal control and membranous nephropathy cohorts is presented in Table 1.MN group showed older age, higher lipid, creatinine and 24h urine protein, lower serum albumin, with lower male proportion.

Table 1
Baseline demographic and clinical characteristics of study participants

Grup	NC	MN
Sample case	N = 8	N = 5
Male sex (%)	8(100%)	3(60%)
Age	37.3	51.8
TCHOL (mmol/l)	4.05	7.42
Scr (umol/l)	101.1	120.4
24-hour urine protein (g/24h)	0	4.72
ALB	39.5	18.26

Limma package in R was used to Identify the DEPs in the subsection of glomeruli in the renal tissue of MN and NC.There are 29DEPs in the subsection of glomeruli.18 of them were up-regulated and 11 were down-regulated(Fig. 2AB).

To decode the biological functions enriched by DEPs, GO enrichment analysis covering biological process (BP), cellular component (CC), and molecular function (MF) was implemented (Fig. 2C). Top enriched BP terms were humoral immune response, blood coagulation, response to oxidative stress and complement activation (including classical complement pathway), which are core pathological events driving glomerular injury in MN. Dominant MF terms contained heme binding, antioxidant activity and peroxidase activity, indicating disrupted redox homeostasis in MN circulation. For CC category, blood microparticle, collagen-containing extracellular matrix and focal adhesion represented the most prominent compartments where DEPs localized, linking circulating protein alterations to glomerular extracellular matrix remodeling.

KEGG pathway enrichment analysis further uncovered signaling cascades perturbed in MN (Fig. 2D). The complement and coagulation cascades pathway exhibited the highest enrichment score, consistent with GO results, followed by folate biosynthesis. Moderately enriched pathways included renin–angiotensin system, cholesterol metabolism and renin secretion, which are tightly associated with renal fibrosis, lipid nephrotoxicity and blood pressure regulation in glomerular diseases.

PPI network uncovered core hub proteins driving MN pathogenesis (Fig. 3AB). Top hubs HP, FGB and C4A dominate complement-coagulation inflammatory cascades. APOE, CLU and AMBP form a lipid homeostasis module regulating podocyte injury. Hemoglobin subunits HBA1, HBB and HBG2 cluster tightly with HP, reflecting systemic oxidative stress. Peripheral nodes like FBLN1 link ECM remodeling to glomerular structural damage. These interconnected hubs coordinate immune activation, lipid disorder and redox imbalance, serving as promising circulating biomarkers for MN(Fig. 3C).

Screening of Diagnostic Biomarkers for MN via Machine Learning Algorithms

Based on protein expression profiles from 5 MN patients and 11 NC subjects, we implemented LASSO logistic regression and RF algorithms to screen and validate potential diagnostic protein biomarkers for MN, with comprehensive results presented in Fig. 4A–D.The RF yielded a total of 18 predictive proteins;LASSO regression identified 6 unique proteins, and RFE-SVM screened 4 unique proteins;A core panel of 3 overlapping proteins was simultaneously captured by all three algorithms, namely HPT, FBLN1, and APOE. These three shared proteins were prioritized for subsequent diagnostic performance verification as the most stable and consensus biomarkers across distinct feature-selection pipelines(Fig. 5A).ROC curve analysis further validated their individual diagnostic performance (Fig. 5B–D): HPT and APOE both attained an AUC of 0.95 (95% CI: 0.8351–1.0), while FBLN1 displayed the optimal AUC of 0.975 (95% CI: 0.9057–1.0). All three shared proteins achieved AUC values exceeding 0.95, confirming their strong capacity to distinguish MN patients from normal controls.

Construction of Weighted Gene Co-Expression Network (WGCNA) and Module-Trait Correlation Analysis

WGCNA was implemented on the protein expression dataset to construct co-expression modules (Fig. 6A–D). We first screened the optimal soft threshold power for scale-free network construction: mean connectivity gradually decreased with rising soft threshold power (Fig. 6A), and a power value of 7 was selected because it yielded a scale-free topology fit $R2 > 0.8$ (Fig. 6B). Based on topological overlap dissimilarity, hierarchical clustering generated a protein dendrogram, and dynamic tree cutting partitioned proteins into multiple distinct co-expression modules annotated by different colors (Fig. 6D). The topological overlap heatmap further illustrated strong intramodular protein correlations visualized as concentrated red blocks, alongside weak intermodule connections, consistent with the module classification from the dendrogram (Fig. 6C). Collectively, a reliable scale-free protein co-expression network was established with well-separated functional modules for downstream trait association analysis of MN.

Module–phenotype correlation analysis was carried out to decode the phenotypic relevance of resolved WGCNA co-expression modules (Fig. 7A). Correlation heatmap outcomes revealed prominent statistically significant associations concentrated in the yellow, brown and turquoise modules; the yellow module exhibited the strongest negative correlation with A4 and A5 phenotypes, while the turquoise module had robust positive linkage to C-series phenotypic indices. Subsequent scatterplots (Fig. 7B) documented significant moderate positive correlations between module membership and trait-based gene significance across the three prioritized modules (all $P < 10 - 20$). Proteins with elevated intramodular connectivity displayed stronger phenotypic trait relevance, solidifying yellow, brown, and turquoise modules as biologically meaningful trait-correlated clusters that complement our previously screened machine learning biomarker candidates.

We detected no overlapping DEPs in the yellow WGCNA module. And the brown module contained the maximal DEPs overlap, with biomarkers APOE, AMBP, BCAM, FBLN1 and CIRBP localized to this module, whereas CLU localized to the turquoise module (Fig. 8A). GO and KEGG enrichment of the brown module (Fig. 8B) highlighted enrichment in kidney injury-relevant processes including wound repair, extracellular matrix remodeling, focal adhesion and ECM–receptor interaction, aligning with core pathological hallmarks of membranous nephropathy. Enrichment results for the turquoise module (Fig. 8C) reflected prevalent involvement in RNA splicing, organelle metabolism, fatty acid turnover and intracellular vesicular transport. Functional discrepancies across the two trait-associated modules indicate brown-module proteins drive glomerular structural remodeling during MN pathogenesis, while turquoise-module members mediate underlying intracellular metabolic and trafficking regulatory programs.

Consistently identified as a core hub protein across hub-protein screening, machine learning feature selection and WGCNA(Table 2), APOE was selected for experimental validation.

Table 2
Summary of hub proteins obtained from PPI network screening, machine learning screening and WGCNA module analysis

Hub-protein	Machine learning	WGCNA
APOE	FBLN1	APOE
FGB	APOE	AMBP
HP	HPT	FBLN1
		BCAM
		CIRBP
		CLU

Experimental Validation of the Candidate Biomarker APOE via IHC and WB

Renal biopsy specimens from enrolled MN and NC participants were instantly placed in 4% paraformaldehyde for IHC sample fixation, with residual fresh tissue snap-frozen in liquid nitrogen and stored at − 80°C to prevent protein degradation for subsequent WB testing. IHC analysis incorporated renal tissues from 2 MN patients and 2 NC subjects; WB utilized specimens from an expanded cohort comprising 6 MN patients and 6 NC subjects.All participants provided written informed consent before sample collection.This study was approved by the Ethics Committee of the 924th Hospital of the Joint Logistics Support Force of the Chinese People's Liberation Army (approval number: Guiyi 2023 [70]).

The MCE-sourced APOE primary antibody (catalog YA1516) was deployed as the detection reagent across both assays, with a unified working dilution of 1:1200 adopted for IHC incubation and WB

membrane probing.

IHC Procedure and Results

Fixed renal tissues underwent routine paraffin embedding, sectioning, antigen retrieval, endogenous peroxidase blockade, overnight primary antibody incubation at 4°C, secondary antibody labeling, DAB chromogenic visualization and hematoxylin counterstaining. Glomerular regions were manually demarcated for morphometric size documentation; glomerular APOE abundance was quantified via H-score, with intergroup disparity assessed by Student's t-test.

The result of IHC images visually illustrated the disparity in glomerular APOE immunoreactivity between the MN and NC cohorts (Figure.9A–B).Glomerular-region annotated IHC micrographs demonstrated stronger APOE immunostaining in MN renal tissue versus NC controls, with the most intense brown DAB signal specifically enriched inside manually traced glomeruli of MN samples. NC glomeruli showed weak baseline APOE staining, corroborating statistically significant APOE upregulation at the glomerular compartment in membranous nephropathy.

Serial glomerular fields from IHC sections were manually screened to count intact glomeruli: 7 evaluable intact glomeruli were harvested from renal biopsy specimens of the two MN patients, while 12 intact glomeruli were identified across biopsies from the two NC subjects(Figure.10). Visual appraisal of DAB chromogenic staining consistently revealed stronger brown APOE immunoreactivity within glomeruli originating from MN samples. Quantitative H-score violin plot analysis corroborated the visual observation, yielding a statistically significant elevation of glomerular APOE staining intensity in the MN group ($p = 0.0035$). These glomerulus-level quantitative findings solidified that APOE protein expression is markedly upregulated at the glomerular compartment in membranous nephropathy.

WB Procedure and Results

Total renal protein was extracted from cryopreserved specimens, followed by protein concentration normalization. Denatured protein samples were separated by SDS-PAGE, transferred onto PVDF membranes, and blocked with non-fat milk. Membranes were probed overnight at 4°C using the aforementioned YA1516 APOE antibody; β-actin acted as the internal loading reference. After secondary antibody incubation and chemiluminescent imaging, band integrated density (IntDen) values were quantified for statistical comparison via Student's t-test.

Western blotting using renal proteins from 6 MN and 6 NC subjects validated APOE expression differences at the bulk tissue level (Fig. 11A–E). Uniform β-actin band intensity confirmed equal sample loading. The 36 kDa APOE bands exhibited visibly higher signal strength in MN samples, which was supported by densitometric IntDen statistics showing a highly significant expression elevation in MN ($P < 0.0001$). These bulk-protein findings align with glomerular IHC results, jointly verifying APOE upregulation in membranous nephropathy renal tissue.

Single-Cell Transcriptomic Profiling and In Silico APOE Knockdown Analysis Based on Dataset GSE241302

We analyzed public single-cell dataset GSE241302 to resolve cell-type-specific transcriptomic shifts upon in silico APOE knockdown. Dot plots and UMAP clustering depicted cell-type marker expression patterns and divergent renal cellular composition between MN and control samples(Fig. 12A-C). Differential expression analysis highlighted PLG as the top upregulated gene, with SLC-family transporters serving as core network hubs(Fig. 13AB). Functional enrichment demonstrated APOE perturbation alters pathways mechanistically tied to MN pathology(Fig. 13CD): impaired glutathione metabolism elevates podocyte oxidative damage, defective xenobiotic detoxification amplifies intrarenal toxin-mediated glomerular injury, and disrupted lipid metabolic signaling accelerates glomerular sclerosis. Tubular transporter transcriptional abnormalities further promote proteinuria onset. Cell-level mechanistic evidence from single-cell sequencing corroborates bulk experimental findings, elaborating how APOE participates in membranous nephropathy pathogenesis via modulation of renal redox homeostasis, metabolite transport and lipid metabolism.

Screening of Candidate Therapeutic Drugs and Validation of APOE-Molecule Docking

Predictive drug activity screening identified eight high-potency BRD-class small molecules with robust predicted APOE-binding affinity (Fig. 14A), with BRD-K76617868 and BRD-K93023739 ranking highest in binding potency. Molecular docking (Fig. 14B) demonstrated stable ligand embedding within APOE's alpha-helical binding groove, sustained by residue-resolved hydrogen-bond interactions. The computational findings pinpoint candidate therapeutic agents capable of targeting pathogenic APOE bioactivity in membranous nephropathy.

Core Mechanistic Findings of APOE in MN Pathogenesis

Through glomerular proteomic profiling, WGCNA, machine learning screening, single-cell transcriptome analysis, in silico gene knockout, molecular docking and experimental validation (IHC, western blot), we identified APOE as a core hub protein driving membranous nephropathy (MN) pathogenesis, and systematically sorted out five downstream pathological pathways mediated by APOE dysregulation(Fig. 15):

Cholesterol & lipid metabolism

APOE forms a lipid homeostasis regulatory module together with CLU and AMBP. Abnormal APOE expression disrupts fatty acid turnover, induces intrarenal lipid accumulation, directly triggers podocyte injury, glomerulosclerosis and lipid-related nephrotoxicity.

Complement & coagulation cascades

APOE interacts with hub proteins HP, FGB and C4A to activate complement and coagulation pathways, boost humoral immune response, and promote glomerular immune complex deposition, which further aggravates glomerular immune injury in MN.

Oxidative stress & glutathione metabolism

Dysregulated APOE reduces glutathione synthesis and antioxidant capacity, elevates reactive oxygen species (ROS) level, causes oxidative damage to podocytes, and facilitates accumulation of renal toxic substances.

ECM remodeling & focal adhesion

Within the WGCNA brown module, APOE cooperates with FBLN1 to remodel extracellular matrix, thicken glomerular basement membrane (GBM), destroy glomerular filtration barrier, and induce renal fibrosis.

Tubular transport & vesicle trafficking

Aberrant APOE alters the expression of SLC family transporters and vesicle trafficking genes, impairs tubular reabsorption function, and sustains persistent proteinuria in MN patients.

Collectively, APOE exerts pathogenic effects via the above five axes, eventually leading to comprehensive MN pathological phenotypes including podocyte injury, immune complex deposition, GBM thickening, tubular dysfunction, proteinuria and renal fibrosis.

Multi-pathway rescue effects of in silico APOE knockdown on MN pathological alterations

We further dissected how APOE knockdown ameliorates MN via four core pathways through transcriptomic comparison between high-APOE MN status and simulated APOE knockdown conditions(Fig. 16):

Glutathione metabolism pathway

Elevated APOE in MN disturbs glutathione synthesis, lowers GSH level, boosts reactive oxygen species (ROS) overproduction and podocyte oxidative damage to induce glomerular injury; APOE knockdown restores glutathione metabolic flux, elevates GSH content, reduces ROS accumulation and protects podocytes from oxidative injury.

Xenobiotic detoxification pathway

Overexpressed APOE suppresses phase I (CYP450) and phase II (UGT, SULT, GST) detoxification reactions, causing intrarenal toxin buildup and glomerular damage; APOE knockdown recovers the activity of detoxification enzymes, accelerates toxin excretion and mitigates renal toxic injury.

Lipid metabolism signaling pathway

High APOE breaks lipid homeostasis, upregulates profibrotic TGF-β/PDGF/NF-κB signaling, leading to cholesterol deposition, lipid peroxidation, mesangial matrix accumulation and glomerulosclerosis; APOE knockdown restrains profibrotic cascades, relieves lipid dysregulation and slows sclerotic progression.

SLC-family tubular transporter pathway

Excessive APOE dysregulates transcription of SLC transporters, impairs tubular reabsorption, triggers proteinuria and worsens glomerular injury; APOE knockdown normalizes SLC transporter expression, recovers tubular reabsorption capacity and reduces urinary protein loss.

Overall, simulated APOE knockdown reverses oxidative stress, toxin retention, lipid dysregulation and proteinuria simultaneously, producing comprehensive renal protective effects for MN.

Discussion

This multi-omics work combining LCM glomerular proteomics, WGCNA, machine learning, single-cell transcriptomics and tissue-level validation identifies APOE as the central driver of MN. We systematically delineate five interconnected APOE-governed pathological axes: podocyte lipid lipotoxicity, complement-coagulation inflammatory activation, glutathione-dependent oxidative stress, extracellular matrix (ECM) remodeling, and tubular solute carrier (SLC) transporter dysfunction. Most contemporary MN omics studies treat lipid metabolic abnormalities as secondary complications of nephrotic-range proteinuria, while our results demonstrate glomerular APOE overexpression is an upstream causal mediator linking all hallmark MN lesions, consistent across bioinformatic screening,IHC,WB and in silico gene knockdown assays.

Lipotoxic podocyte injury driven by APOE

Recent studies generalized that lipid overload induces podocyte mitochondrial dysfunction, ROS burst and cytoskeletal damage across all proteinuric nephropathies[26], our single-cell transcriptomics and in silico APOE knockdown verified that elevated APOE suppresses glutathione metabolism, amplifies podocyte oxidative stress, forming a lipotoxicity-mitochondrial damage vicious cycle described by Ge et al[27]. Garavaglia et al.summarized that APOE aberrations mediate both systemic dyslipidemia and intrarenal lipid deposition across rare and common glomerular diseases[28]; Another two studies focusing on lipoprotein glomerulopathy (LPG) highlighted genetic APOE defects as the primary pathogenic driver: the meta-analysis by Li et al. demonstrated that germline APOE mutations underpin massive glomerular lipoprotein deposition[29], and Liu et al. further validated that the APOE Chicago variant triggers early-onset LPG with severe lipid-mediated glomerular damage[30]. In summary, integrating existing research with our findings, APOE plays a central role in glomerular injury mediated by lipid metabolic disorders. Our study confirms that in MN, the abnormal overexpression of APOE disrupts lipid homeostasis in podocytes, triggering intracellular lipid overload and lipotoxic injury, which ultimately leads to the dysfunction of the filtration barrier. This discovery not only elucidates the critical role of

APOE in the pathogenesis of MN but also provides strong evidence for its potential as a diagnostic biomarker and therapeutic target, highlighting the significant value of APOE in the precision treatment of MN.

APOE bridges complement-coagulation cascades to amplify glomerular immune injury

Our glomerular LCM-based proteomic study verified that APOE acts as a molecular bridge interconnecting complement and coagulation cascades to amplify glomerular immune injury in MN. This core mechanism echoes recent research on C3 glomerulopathy (C3G) documented in the reference literature, while evident disease-specific distinctions exist between MN and C3G[31]. And Tavares et al.reported massive APOE accumulation within glomerular dense deposits in dense deposit disease (DDD, a subtype of C3G). Pathogenic APOE simultaneously binds C3b and factor Xa to assemble ternary complexes, triggering synergistic activation of the alternative complement pathway and coagulation cascade[32]. Hurdogan et al.further validated that APOE immunohistochemical staining reliably distinguishes DDD from C3 glomerulonephritis, confirming glomerular APOE deposition as a signature marker of concurrent complement-coagulation activation[33].Consistent with these C3G findings, our PPI and KEGG enrichment results validated that APOE interacts closely with complement hub proteins C4A, coagulation mediator FGB and inflammatory HP in MN glomeruli, forming a central complex that amplifies classical complement pathway activation and glomerular immune complex deposition.our findings deepen the mechanistic understanding of MN by unravelling the APOE-complement-coagulation amplification loop. Furthermore, molecular docking screened candidate small-molecule compounds targeting APOE, offering novel therapeutic strategies to block complement-coagulation cross-talk and mitigate glomerular immune injury for MN clinical intervention.

APOE aggravates podocyte oxidative stress

Existing literature has confirmed the tight linkage between APOE dysregulation, lipid disturbance and renal oxidative stress, which supports our multi-pathway mechanism of APOE-mediated MN injury. Hong et al. reported that ApoE knockout mice under high-fat diet develop severe renal damage through RAGE-dependent inflammatory and oxidative cascades[34], while Qian et al.further verified that lipid overload triggers excessive reactive oxygen species (ROS) accumulation and renal lesions in APOE-deficient animals[35]. and Pei et al. demonstrated that restoring antioxidant capacity could reverse hyperlipidemia-related kidney injury driven by abnormal APOE function[36].Indicated that apolipoproteins are core regulators of renal lipid metabolism and redox balance[37].Consistent with these findings, our single-cell transcriptomic and in silico APOE knockdown analyses revealed that elevated APOE in MN suppresses glutathione metabolism, impairs antioxidant defense and aggravates podocyte oxidative damage, forming a synergistic pathogenic loop together with complement-coagulation overactivation. While prior animal studies mainly focused on hyperlipidemic renal injury in ApoE$^{-/-}$ models, our work extends this redox regulatory axis to human autoimmune MN. We illustrated that APOE aggravates oxidative stress, amplifying glomerular immune injury.

APOE mediates ECM remodeling

Our PPI and WGCNA module analysis positioned APOE within the brown module enriched in ECM remodeling pathways, where APOE interacts with FBLN1 to drive glomerular basement membrane thickening and glomerular structural destruction. Published studies have uncovered the profibrotic role of APOE in renal lesions, which aligns well with our WGCNA and proteomic results regarding ECM remodeling in MN. Nishimura et al.found that combined deletion of eNOS and ApoE drastically promotes renal fibrosis and cellular senescence after kidney injury, highlighting aberrant APOE as a driver of progressive fibrotic damage[38]. Fazeli and Javanmard further integrated machine learning and CRISPR editing to confirm that APOE mediates lipid metabolism-related renal fibrosis, establishing a causal link between dysregulated APOE and ECM overaccumulation[39].Our findings refine the APOE-fibrosis axis specific to human MN, bridging early immune injury and late glomerular sclerosis uncovered by prior animal research. APOE-FBLN1 interaction directly drives GBM lesions, and screened APOE-targeted compounds may simultaneously block immune activation and fibrosis. Further in vivo trials are needed to verify their renoprotective anti-fibrotic efficacy for progressive MN.

APOE impairs tubular SLC transporters

In our study, in silico APOE knockdown analysis revealed that overexpressed APOE disturbs the transcription of multiple SLC transporters, impairs tubular reabsorption and sustains persistent proteinuria. In line with our study,accumulating evidence has linked APOE to tubular SLC transporters and proteinuria, Wu et al.proved APOE variants interfere with SLC transporter function in dyslipidemic populations[40], while Zaki et al. identified co-altered APOE and SLC family transcripts in chronic kidney disease, implying a regulatory connection between APOE and tubular transport[41]. Gu et al. captured disrupted tubular transcriptomes in primary MN[42], and Faivre et al. confirmed glomerular proteinuria triggers profound tubular dysfunction, with megalin (LRP2, a core SLC-related transporter) acting as a critical mediator of tubular injury [43, 44].Distinct from previous observational reports, our work establishes a causal link between APOE overexpression and SLC transporter dysfunction specifically in MN, bridging glomerular APOE-mediated immune injury to downstream tubular proteinuria. Targeting APOE may simultaneously restore tubular reabsorption and mitigate glomerular lesions. Further animal experiments are required to validate whether APOE inhibition recovers SLC expression and relieves persistent proteinuria in MN.

APOE acts as MN diagnostic biomarker

Recent biomarker-oriented proteomic and pathological studies suggested that APOE exerts promising auxiliary diagnostic value for MN.A rare case report described APOE mutation-driven MN-like glomerular deposition, highlighting APOE's pathological deposition capacity within glomeruli[45]. Previtali et al.profiled serum proteome of idiopathic MN and detected broad apolipoprotein dysregulation[46].Our study integrated glomerular LCM proteomics, three machine learning algorithms and histological validation (IHC/WB) to confirm glomerular APOE elevation as a high-performance MN biomarker (AUC =

0.95).we linked APOE biomarker potency to its multi-pathway pathogenic functions in MN, bridging diagnostic marker screening and mechanistic exploration.

Concluding

This multi-omics study identified APOE as a core pathogenic hub and high-performance glomerular biomarker for MN (AUC>0.95), verified by IHC and WB. Glomerular APOE overexpression triggers podocyte injury, immune inflammation, oxidative stress, ECM remodeling and tubular dysfunction via five interrelated pathways; virtual APOE knockdown reversed these lesions. Two high-affinity APOE-targeted small molecules were screened by molecular docking. This work complements the defects of anti-PLA2R antibody and reveals APOE as an upstream driver of MN lipid disorder rather than a secondary outcome. Though restricted by small samples and insufficient functional verification, it provides novel theoretical evidence for MN precise diagnosis and targeted therapy, laying groundwork for subsequent cohort expansion and in vivo functional validation.

Limitations

This study has several notable limitations restricting translational application of our findings. First, the sample size is relatively small. The discovery proteomic cohort only included 5 MN patients and 8 normal controls, and IHC validation merely adopted 2 cases per group. No independent external large cohort was applied to verify the diagnostic panel of APOE, FBLN1 and HPT. Besides, we failed to stratify patients by PLA2R status, disease risk grade or proteinuria severity, leaving the subgroup-specific expression pattern of glomerular APOE unclear. Second, all mechanistic exploration relied on in silico APOE knockdown simulation based on public single-cell dataset GSE241302. We lacked in vitro podocyte/tubular cell functional tests and ApoE-modified animal models to confirm the causal relationship between APOE and five pathological axes. Third, two candidate APOE-targeted small molecules were only screened via molecular docking without cellular pharmacodynamic and in vivo therapeutic validation. We only detected tissue APOE rather than serum and urinary APOE for non-invasive biomarker exploration, and long-term follow-up data were absent to evaluate the prognostic value of APOE.

Future Work

Future research will systematically supplement and validate the current conclusions. First, a multi-center large independent cohort will be recruited with stratified subgroups including PLA2R-positive/negative and low/medium/high-risk MN patients. Glomerular, serum and urinary APOE will be simultaneously quantified to construct a combined diagnostic model integrated with anti-PLA2R antibody. Longitudinal clinical follow-up will be conducted to explore the correlation between APOE level and renal endpoints such as proteinuria remission and ESRD progression. Second, APOE overexpression and knockdown podocyte cell models as well as ApoE transgenic/knockout MN animal models will be established to verify the direct regulatory effects of APOE on lipid metabolism, oxidative stress and ECM remodeling. Third, cellular intervention and in vivo animal experiments will be performed to test the renoprotective

efficacy and biosafety of BRD-K76617868 and BRD-K93023739. We will further investigate upstream transcriptional and epigenetic mechanisms driving APOE upregulation and develop non-invasive diagnostic tools based on circulating APOE for clinical translation.

Abbreviations

Full Name
AMBP
Alpha-1-Microglobulin/Bikunin Precursor
APOE
Apolipoprotein E
AUC
Area Under the Receiver Operating Characteristic Curve
BCAM
Basal Cell Adhesion Molecule
BCA
Bicinchoninic Acid
BP
Biological Process
BRD
Broad Institute Compound Library
CC
Cellular Component
CIRBP
Cold Inducible RNA Binding Protein
CLU
Clusterin
DAB
3,3'-Diaminobenzidine
DDA
Data-Dependent Acquisition
DEGs
Differentially Expressed Genes
DEPs
Differentially Expressed Proteins
DIA
Data-Independent Acquisition
ECM
Extracellular Matrix
ECL

Enhanced Chemiluminescence
ESRD
End-Stage Renal Disease
FC
Fold Change
FFPE
Formalin-Fixed Paraffin-Embedded
FBLN1
Fibulin 1
FGB
Fibrinogen Beta Chain
GAPDH
Glyceraldehyde-3-Phosphate Dehydrogenase
GBM
Glomerular Basement Membrane
GO
Gene Ontology
GSH
Glutathione
GSSG
Oxidized Glutathione
HP
Haptoglobin
HPT
Haptoglobin
HRP
Horseradish Peroxidase
H-score
Histological Score
IHC
Immunohistochemistry
KEGG
Kyoto Encyclopedia of Genes and Genomes
KDIGO
Kidney Disease: Improving Global Outcomes
LASSO
Least Absolute Shrinkage and Selection Operator
LCM
Laser Capture Microdissection
LC-MRM-MS

Liquid Chromatography-Multiple Reaction Monitoring Mass Spectrometry
LPG
Lipoprotein Glomerulopathy
LRP2
Low-Density Lipoprotein Receptor-Related Protein 2
MF
Molecular Function
MENTOR
Rituximab vs Cyclosporine for Membranous Nephropathy Clinical Trial (trial name)
MN
Membranous Nephropathy
MRM
Multiple Reaction Monitoring
NC
Normal Control
PCA
Principal Component Analysis
PDB
Protein Data Bank
PPI
Protein-Protein Interaction
PLA2R
Phospholipase A2 Receptor
PVDF
Polyvinylidene Difluoride
RAAS
Renin-Angiotensin-Aldosterone System
RI-CYCLO
Rituximab and Cyclophosphamide for Membranous Nephropathy Clinical Trial (trial name)
RIPA
Radio-Immunoprecipitation Assay
ROC
Receiver Operating Characteristic Curve
RF
Random Forest
RFE-SVM
Recursive Feature Elimination-Support Vector Machine
ROS
Reactive Oxygen Species
Scr

Serum Creatinine
SLC
Solute Carrier
SDS-PAGE
Sodium Dodecyl Sulfate-Polyacrylamide Gel Electrophoresis
THSD7A
Thrombospondin Type 1 Domain Containing 7A
TCHOL
Total Cholesterol
UMAP
Uniform Manifold Approximation and Projection
WB
Western Blot
WGCNA
Weighted Gene Co-expression Network Analysis
Z-score
Standard Score

Declarations

Ethics Approval and Consent to Participate

This study was approved by the Ethics Committee of Shenzhen People's Hospital (approval number: LL-KY-2020167, KY-2020-034) and the Ethics Committee of the 924th Hospital of Joint Logistic Support Force of PLA (approval number: Guiyi 2023 [70]). All enrolled membranous nephropathy patients and kidney transplant donor subjects provided written informed consent before renal biopsy tissue collection.

Competing Interests

The authors declare that there are no conflicts of interest related to this study. No commercial companies or pharmaceutical institutions participated in the design of the research, sample collection, data analysis, manuscript writing or decision to submit this article for publication. None of the authors hold patents related to APOE-targeted small-molecule compounds described in this work.

Funding:

Guangxi Natural Science Foundation (No. 2024GXNSFAA010301); Shenzhen Science and Technology Program(NO.GJHZ20220913142614027); Shenzhen Science and Technology

Program(No.JCYJ20230807112359022); Taizhou Science and Technology Bureau (NO.23ywa60)

Author Contribution

Chang Lu was mainly responsible for drafting and revising the full manuscript, organizing all figures and supplementary materials. Donge Tang focused on proteomic experiments and multi-omics bioinformatic analysis. Guang Hu completed molecular verification tests including IHC, WB and molecular docking simulation. Hualin Ma, Guimian Zou and Shenping Xie took charge of clinical sample recruitment and tissue specimen processing. Jingjing Dong, Zhifeng Luo and Yaoshuang Zou assisted in literature collection and partial data validation. Corresponding authors Yong Dai, Huaizhou Chen and JingSheng Ma conceived the research framework, proposed the core research hypothesis, secured project funding, supervised all experimental and analytical work, finalized the manuscript, and took full responsibility for the integrity of all research results.

Acknowledgements

The authors sincerely thank all patients and kidney donors who provided renal tissue samples for this research. We appreciate the technical support from the pathology department of Shenzhen People's Hospital for FFPE tissue sectioning and immunohistochemical detection. We also acknowledge the public GEO database for providing single-cell RNA-seq dataset GSE241302, and the open-source R packages and AutoDock Vina software that supported all bioinformatic and molecular docking analyses.

Data Availability

We generated original LC-MRM-MS proteomic data from laser-captured glomerular FFPE renal tissues of 5 membranous nephropathy patients and 8 normal controls in this study. The raw proteomic data have not been deposited in public repositories yet but can be available from the corresponding author upon reasonable formal request. In addition, we utilised the public single-cell RNA-seq dataset GSE241302 downloaded from NCBI Gene Expression Omnibus (GEO) database for in-silico gene-knockdown simulation and downstream bioinformatic analysis. All R scripts used for multi-omics bioinformatics analyses, molecular docking files of BRD compound library are preserved on our local research server and can also be accessed by request to the corresponding author. No custom-generated clinical sequencing data were submitted to public databases in the current work. All data usage complies with data access rules of public database and institutional research requirements.

References

1. Efe O, So PNH, Anandh U, et al. An Updated Review of Membranous Nephropathy[J]. Indian J Nephrol. 2024;34(2):105–18.

2. Wang M, Yang J, Fang X et al. Membranous nephropathy: pathogenesis and treatments[J]. MedComm (2020), 2024,5(7):e614.
3. Caravaca-Fontán F, Yandian F, Fervenza FC. Updated diagnostic and therapeutic management for membranous nephropathy[J]. Curr Opin Nephrol Hypertens. 2025;34(1):23–32.
4. Bharati J, Waguespack DR, Beck LHJ. Membranous Nephropathy: Updates on Management[J]. Adv Kidney Dis Health. 2024;31(4):299–308.
5. Fervenza FC, Appel GB, Barbour SJ, et al. Rituximab or Cyclosporine in the Treatment of Membranous Nephropathy[J]. N Engl J Med. 2019;381(1):36–46.
6. Sethi S, Fervenza FC. Membranous nephropathy-diagnosis and identification of target antigens[J]. Nephrol Dial Transpl. 2024;39(4):600–6.
7. Hou W, Shi S, Yan Z, et al. Trends and the Role of Gene-Environment Interactions in Idiopathic Membranous Nephropathy in Northern China[J]. Am J Nephrol. 2025;56(2):148–57.
8. Laurin L, Helmuth M, Almaani S, et al. Risk Factors for Disease Progression for Adults and Children With Membranous Nephropathy in the Cure Glomerulonephropathy Network (CureGN)[J]. Kidney Int Rep. 2025;10(6):1917–28.
9. Scolari F, Delbarba E, Santoro D, et al. Rituximab or Cyclophosphamide in the Treatment of Membranous Nephropathy: The RI-CYCLO Randomized Trial[J]. J Am Soc Nephrol. 2021;32(4):972–82.
10. Shah M, DeLaat A, Cavanaugh C. Treatment of membranous nephropathy: Perspectives on current and future therapies[J]. Front Nephrol. 2023;3:1110355.
11. Choi J, Chin HJ, Lee H, et al. Effect of immunosuppressive agents on clinical outcomes in idiopathic membranous nephropathy[J]. Kidney Res Clin Pract. 2024;43(5):635–47.
12. Russo I, Vargas-Brochero MJ, Cara A, et al. Cancer Incidence and Risk Factors in PLA2R-Associated Membranous Nephropathy[J]. Mayo Clin Proc. 2026;101(4):582–91.
13. Ma S, Chang M, Zhang D, et al. The lipid-podocyte axis: emerging clues in membranous nephropathy pathogenesis[J]. Front Med (Lausanne). 2026;13:1722758.
14. Lu Z, Liu C, Wu Q, et al. High-coverage targeted lipidomics could reveal lipid alterations and evaluate therapeutic efficacy of membranous nephropathy[J]. Nutr Metab (Lond). 2022;19(1):68.
15. Deleersnijder D, Callemeyn J, Arijs I, et al. Current Methodological Challenges of Single-Cell and Single-Nucleus RNA-Sequencing in Glomerular Diseases[J]. J Am Soc Nephrol. 2021;32(8):1838–52.
16. Huang S, Sheng X, Susztak K. The kidney transcriptome, from single cells to whole organs and back[J]. Curr Opin Nephrol Hypertens. 2019;28(3):219–26.
17. Stojanowski J, Gołębiowski T, Musiał K. Artificial Intelligence in Nephrology-State of the Art on Theoretical Background, Molecular Applications, and Clinical Interpretation[J]. Int J Mol Sci, 2026,27(3).
18. Dong B, Liu X, Yu S. Utilizing machine learning algorithms to identify biomarkers associated with diabetic nephropathy: A review[J]. Med (Baltim). 2024;103(8):e37235.

19. Chen Q, Wang G, Zhao R, et al. TIMP4 as a Potential Complementary Biomarker and Therapeutic Target in Membranous Nephropathy: A Multi-Omics Investigation with Clinical Validation[J]. J Inflamm Res. 2025;18:14755–69.
20. Zhang PN, Tang JY, Yang KZ, et al. Integrated Network Pharmacology Analysis and Experimental Validation to Investigate the Molecular Mechanism of Triptolide in the Treatment of Membranous Nephropathy[J]. Drug Des Devel Ther. 2022;16:4061–76.
21. Säemann MD, Odler B, Windpessl M, et al. [Diagnosis and therapy of membranous nephropathy-2023][J]. Wien Klin Wochenschr. 2023;135(Suppl 5):648–55.
22. Filippone EJ, Farber JL. Contemporary review of primary membranous nephropathy[J]. Front Immunol. 2026;17:1836347.
23. Cai N, Zhu S, Huang J, et al. Rituximab, tacrolimus, cyclophosphamide and cyclosporin in primary membranous nephropathy with nephrotic syndrome: comparison of safety profiles, effect on remission rate, 24-h urinary total protein, serum albumin, and serum creatinine levels using network meta-analysis[J]. Int Urol Nephrol. 2025;57(11):3733–50.
24. Dong J, Zheng F, Liu F, et al. Global-feature of autoimmune glomerulonephritis using proteomic analysis of laser capture microdissected glomeruli[J]. Front Immunol. 2023;14:1131164.
25. Shi M, Wang Y, Zhang H, et al. Single-cell RNA sequencing shows the immune cell landscape in the kidneys of patients with idiopathic membranous nephropathy[J]. Front Immunol. 2023;14:1203062.
26. Sun Y, Cui S, Hou Y, et al. The Updates of Podocyte Lipid Metabolism in Proteinuric Kidney Disease[J]. Kidney Dis (Basel). 2021;7(6):438–51.
27. Ge M, Fontanesi F, Merscher S, et al. The Vicious Cycle of Renal Lipotoxicity and Mitochondrial Dysfunction[J]. Front Physiol. 2020;11:732.
28. Garavaglia C, Ossoli A, Gomaraschi M. Lipids in kidney diseases: from systemic imbalance to intrarenal alterations of cellular lipid metabolism in rare and common kidney diseases[J]. J Mol Med (Berl). 2026;104(1):46.
29. Li M, Li Y, Liu Y, et al. An Updated Review and Meta Analysis of Lipoprotein Glomerulopathy[J]. Front Med (Lausanne). 2022;9:905007.
30. Liu Y, Cheng Y, Wen Y, et al. A case report of youth-onset lipoprotein glomerulopathy with APOE Chicago mutation[J]. BMC Nephrol. 2024;25(1):87.
31. Madden B, Singh RD, Haas M, et al. Apolipoprotein E is enriched in dense deposits and is a marker for dense deposit disease in C3 glomerulopathy[J]. Kidney Int. 2024;105(5):1077–87.
32. Tavares J, Caravaca-Fontán F, Praga M. Apolipoprotein E in dense deposits: a parting of the ways in C3 glomerulopathy[J]. Clin Kidney J. 2024;17(6):sfae161.
33. Hurdogan O, Mirioglu S, Dirim AB, et al. Apolipoprotein E Immunostaining Has Diagnostic Utility in Differentiating Dense Deposit Disease and C3 Glomerulonephritis: Clone-Based Evaluation of D719N, EP1373Y, and 1B2C9[J]. Mod Pathol. 2025;38(12):100874.

34. Hong Y, Hu Y, Sun Y, et al. High-fat diet caused renal damage in ApoE(-/-) mice via the activation of RAGE-mediated inflammation[J]. Toxicol Res (Camb). 2021;10(6):1171–6.
35. Qian C, Yang Q, Guo L, et al. Exercise reduces hyperlipidemia-induced kidney damage in apolipoprotein E-deficient mice[J]. Exp Ther Med. 2021;21(2):153.
36. Pei Z, Li Y, Yao W, et al. NAD(+) Protects against Hyperlipidemia-induced Kidney Injury in Apolipoprotein E-deficient Mice[J]. Curr Pharm Biotechnol. 2024;25(4):488–98.
37. Pan X. The Roles of Fatty Acids and Apolipoproteins in the Kidneys[J]. Metabolites, 2022,12(5).
38. Nishimura K, Taguchi K, Kishi S, et al. Dual disruption of eNOS and ApoE gene accelerates kidney fibrosis and senescence after injury[J]. Biochem Biophys Res Commun. 2021;556:142–8.
39. Fazeli SA, Javanmard A. Integrative machine learning and CRISPR/Cas9 analysis reveals the role of APOE in lipid metabolism-associated kidney fibrosis[J]. Mol Med, 2026.
40. Wu X, Cai Y, Su Y, et al. Effects of apolipoprotein E and solute carrier organic anion transporter family member 1B1 gene polymorphisms on statin efficacy and safety in dyslipidemic patients[J]. Pharmacogenet Genomics. 2026;36(4):151–6.
41. Zaki EA, Afifi SM, Ammar NM, et al. Assembled human microbiome and metabolome in chronic kidney disease: Dysbiosis a double-edged sword interlinking Circ-YAP1, Circ-APOE & Circ-SLC8A1[J]. Toxicol Rep. 2025;14:102058.
42. Gu Q, Wen Y, Cheng X, et al. Integrative profiling of untreated primary membranous nephropathy at the single-cell transcriptome level[J]. Clin Kidney J. 2024;17(7):sfae168.
43. Faivre A, Bugarski M, Rinaldi A, et al. Spatiotemporal Landscape of Kidney Tubular Responses to Glomerular Proteinuria[J]. J Am Soc Nephrol. 2024;35(7):854–69.
44. Kukida M, Sawada H, Daugherty A, et al. Megalin: A bridge connecting kidney, the renin-angiotensin system, and atherosclerosis[J]. Pharmacol Res. 2020;151:104537.
45. Koshino A, Takaeda C, Matsuno T, et al. Membranous Nephropathy-Like Apolipoprotein E Deposition Disease with Apolipoprotein E Toyonaka and Homozygous Apolipoprotein E2/2 without Dyslipidemia, with Characteristic Electron-Dense Deposits[J]. Case Rep Nephrol Dial. 2022;12(2):96–104.
46. Previtali P, Pagani L, Risca G, et al. Towards the Definition of the Molecular Hallmarks of Idiopathic Membranous Nephropathy in Serum Proteome: A DIA-PASEF Approach[J]. Int J Mol Sci. 2023;24(14):11756.

Figures

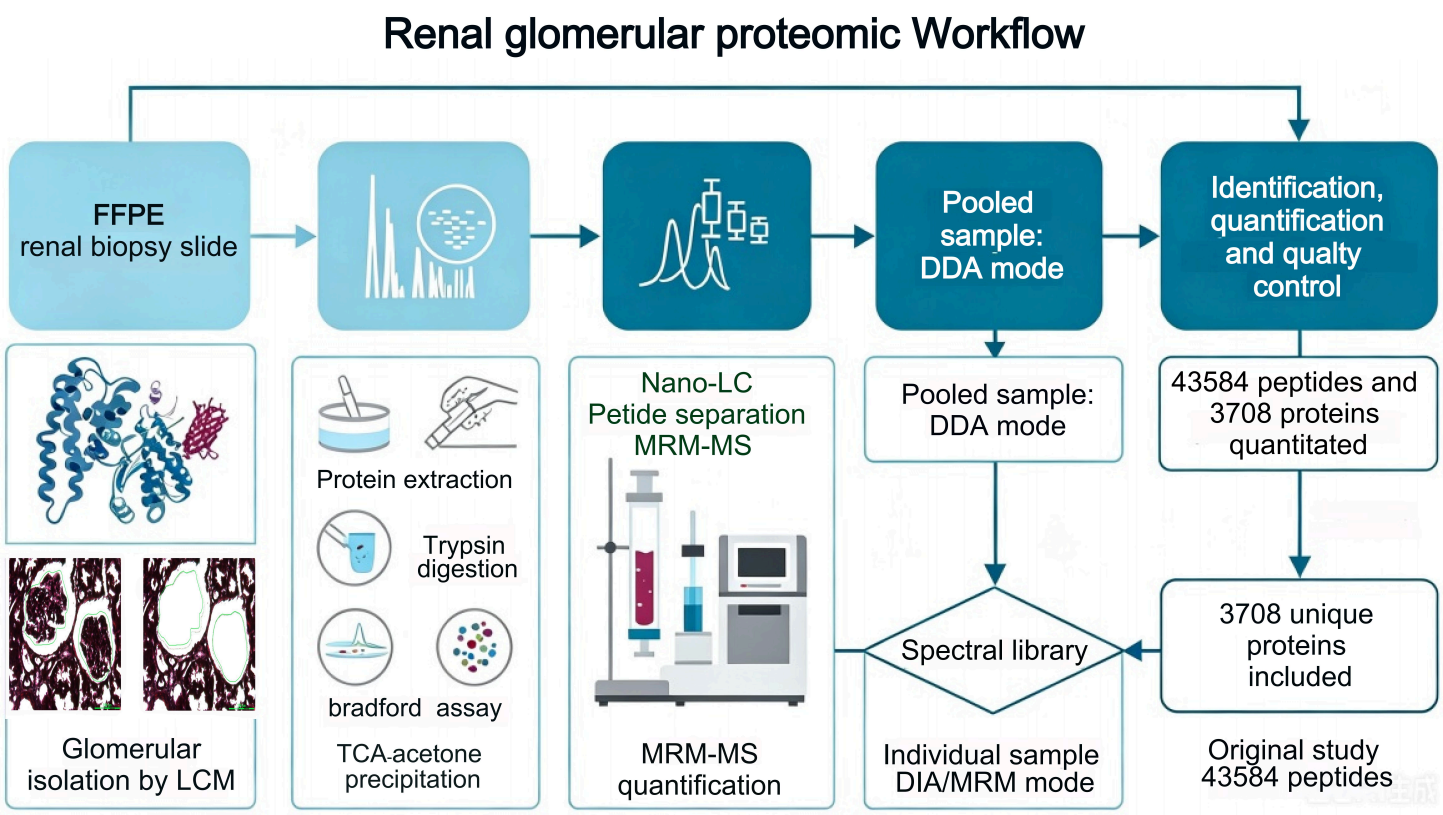


Figure 1

Workflow of renal glomerulus proteomic analysis using FFPE renal biopsy specimens

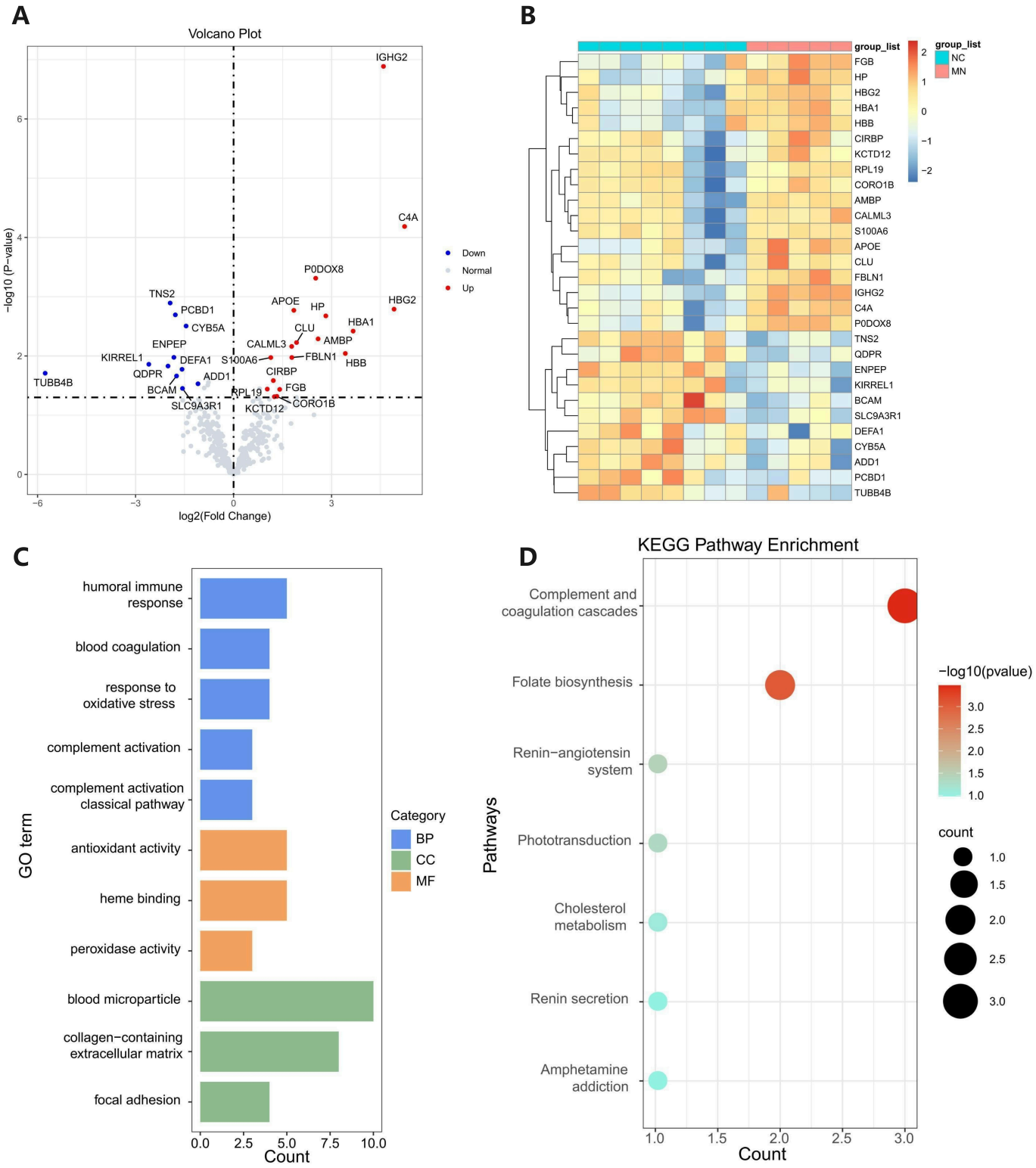


Figure 2

Differential expression and functional enrichment analysis of glomerular proteomes in MN versus control samples(A) Volcano plot marking upregulated (red), downregulated (blue), and non-significant (gray) proteins; major differentially expressed proteins are annotated. (B) Expression heatmap with hierarchical clustering of differentially expressed proteins across NC and MN cohorts. (C) GO enrichment grouped by biological process, cellular component, molecular function. (D) KEGG pathway

enrichment, with bubble color indicating statistical significance and bubble size representing enriched gene quantity.

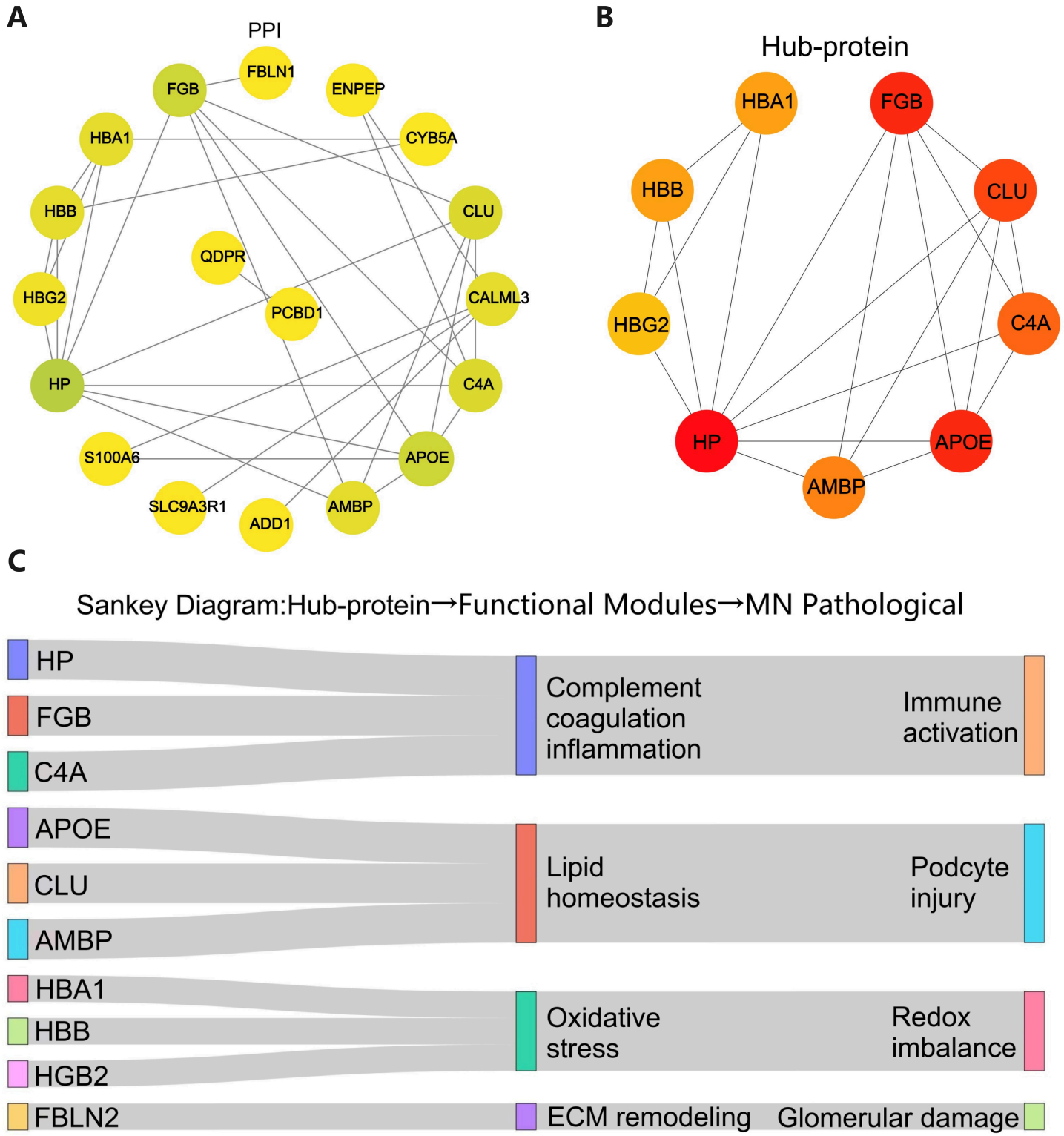


Figure 3

PPI network, hub protein identification and functional pathway mapping for MN-related differentially expressed proteins(A) Global PPI network of differential proteins. (B) Extracted hub protein subnetwork,

node color denotes hub importance. (C) Sankey flow chart showing how hub proteins act via distinct functional modules to trigger typical MN pathological outcomes including immune activation, podocyte injury, redox imbalance and glomerular damage.

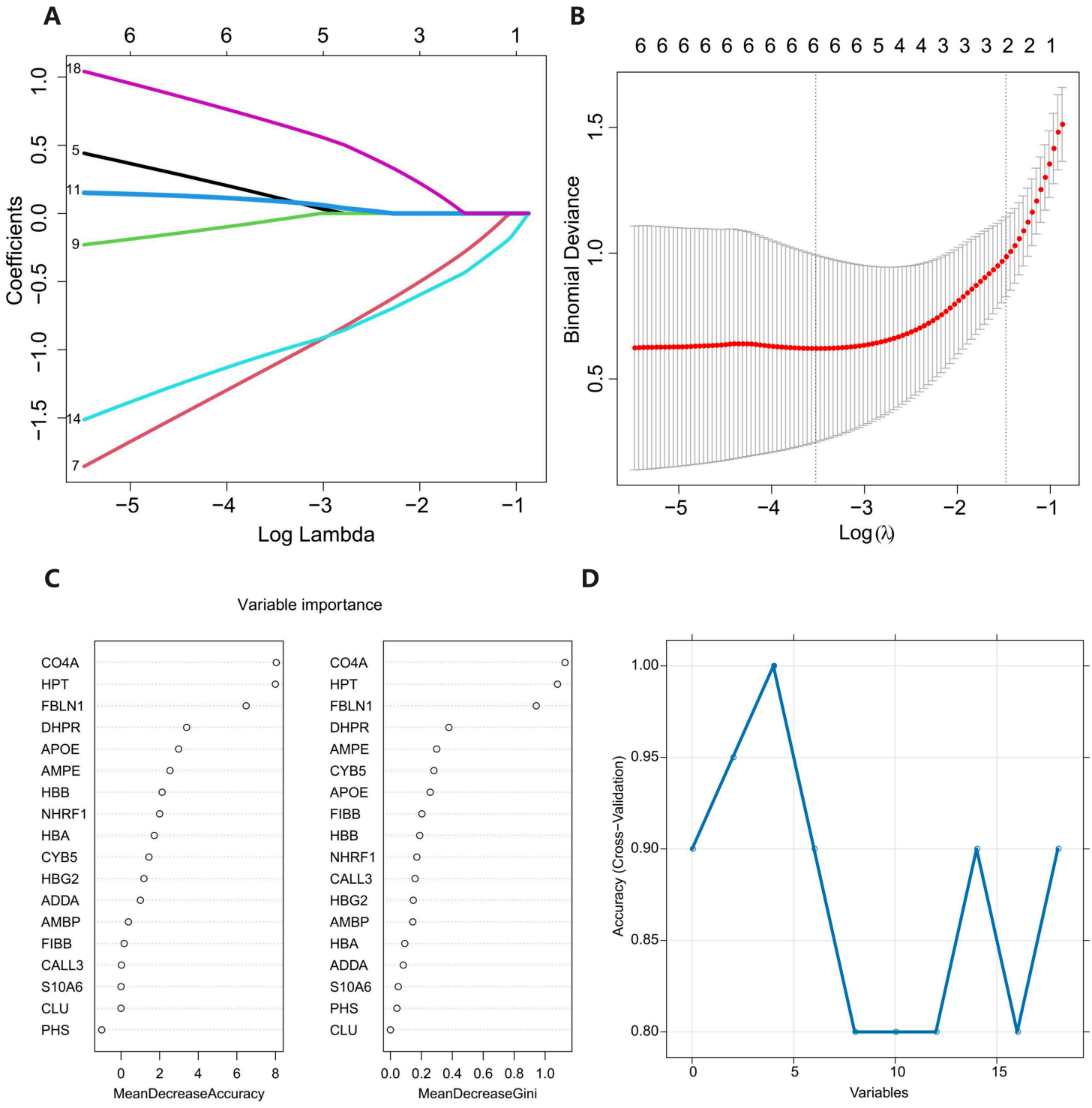


Figure 4

Machine learning screening of diagnostic protein biomarkers(A) LASSO regression coefficient trajectories against log(λ). (B) Binomial deviance cross-validation to determine optimal regularization

parameter. (C) Random forest variable importance evaluated by Mean Decrease Accuracy and Mean Decrease Gini. (D) Cross-validation accuracy across different variable inclusion numbers for model optimization.

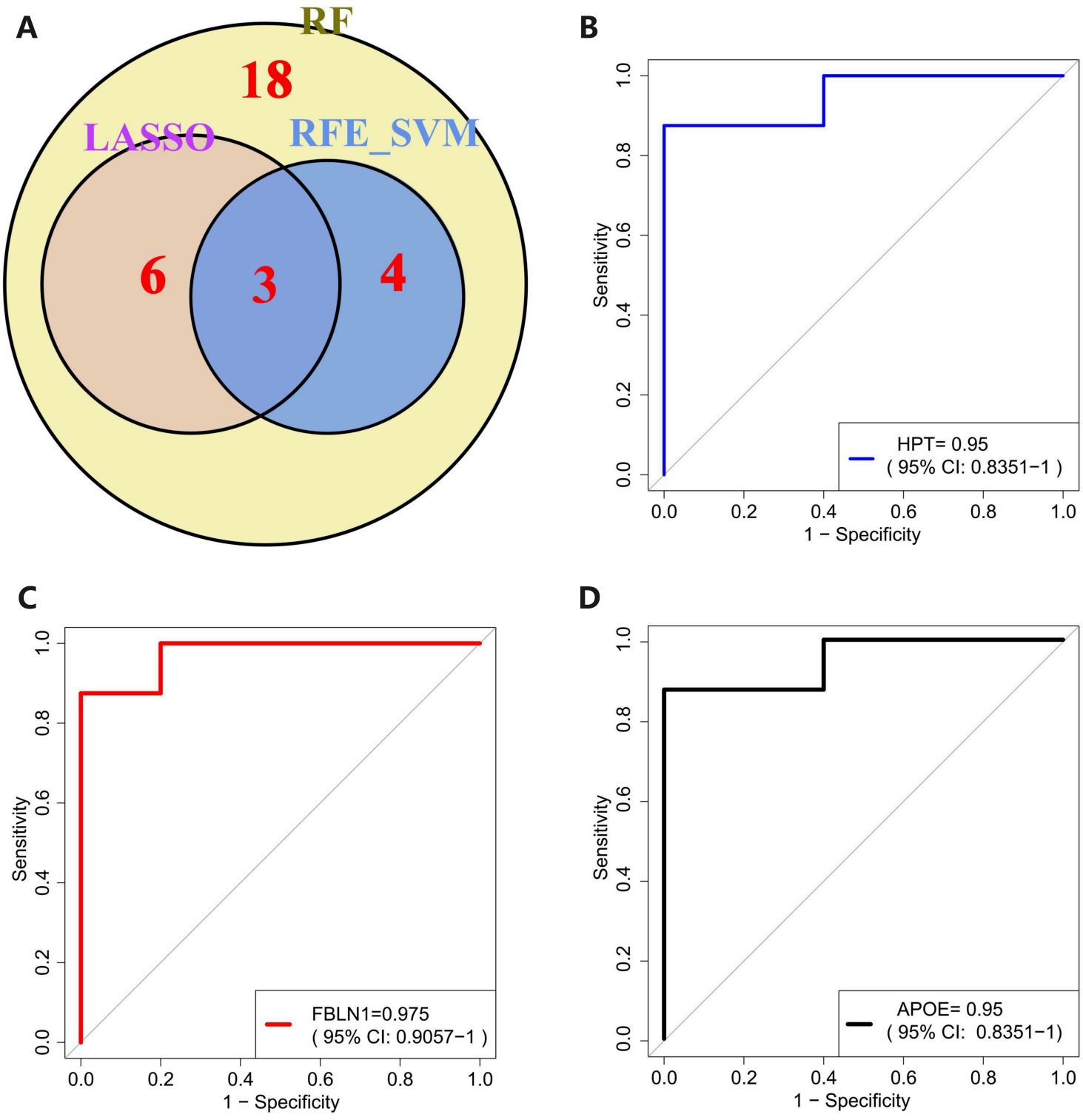


Figure 5

Feature screening and diagnostic efficacy evaluation of candidate proteins(A) Venn diagram showing feature counts screened by RF, LASSO and RFE_SVM algorithms. (B-D) ROC curves quantifying the

diagnostic AUC and 95% CI of HPT, FBLN1 and APOE respectively.

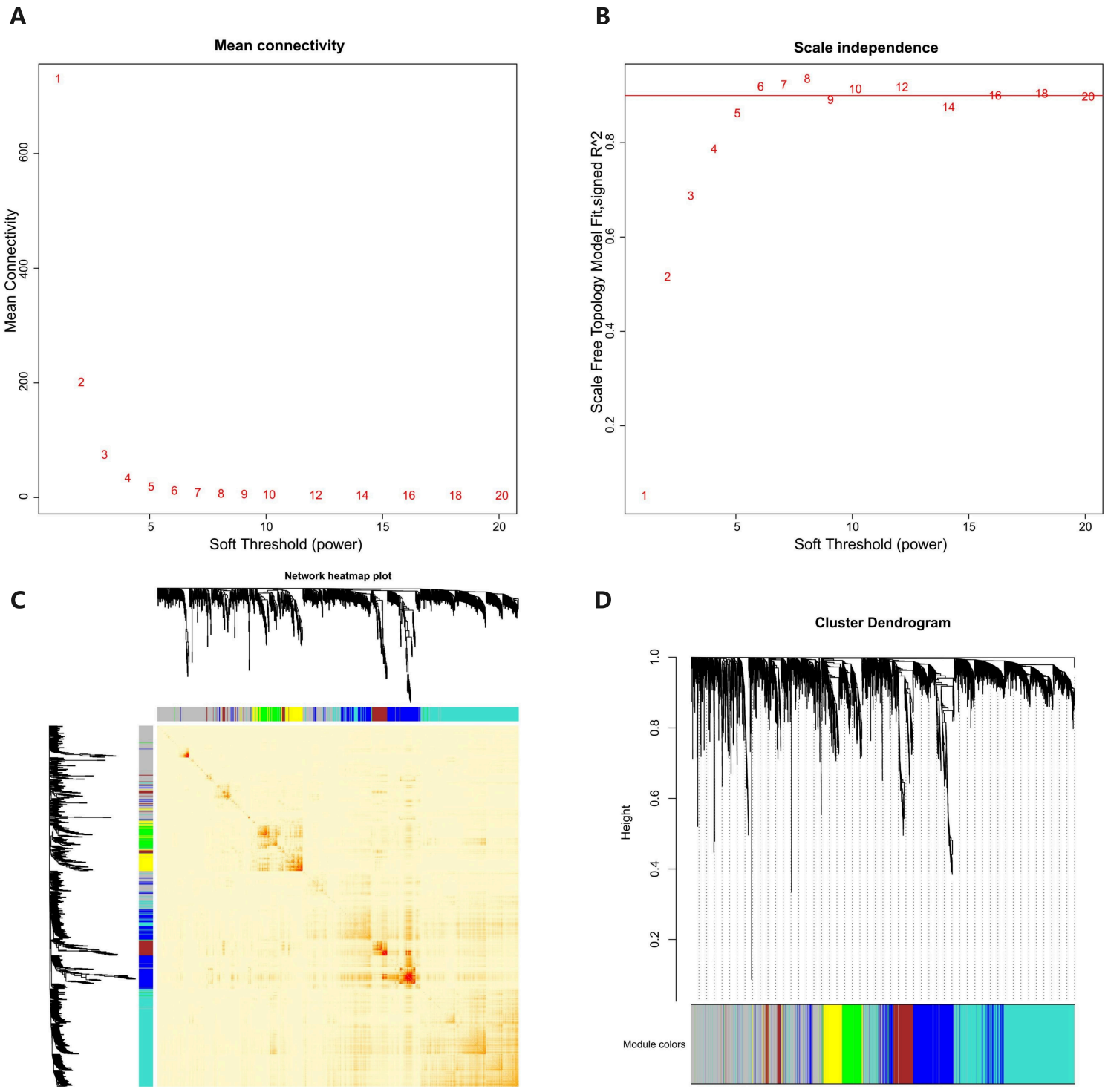


Figure 6

(A) Mean connectivity under different soft threshold powers. (B) Scale-free model fitness for soft threshold selection. (C) Topological overlap heatmap of the protein co-expression network. (D) Protein hierarchical clustering dendrogram and module color annotation for co-expression module partitioning.

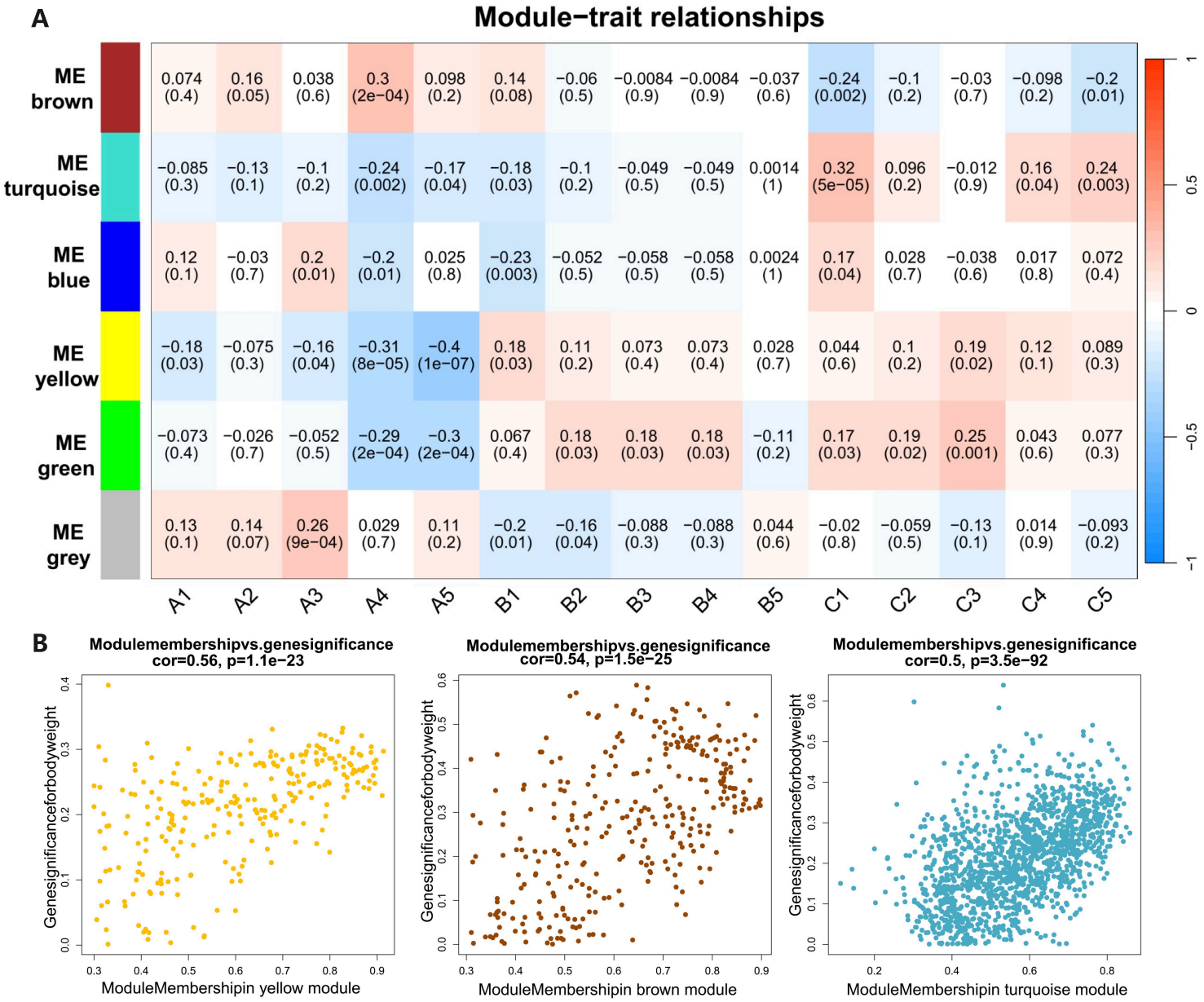


Figure 7

Module-trait correlation and internal gene relevance verification of WGCNA modules(A) Heatmap displaying Pearson correlation and P-value between each module eigengene and clinical phenotypes. (B) Scatter plots of module membership versus gene significance for three key modules, with annotated correlation and P values to validate module robustness for target traits.

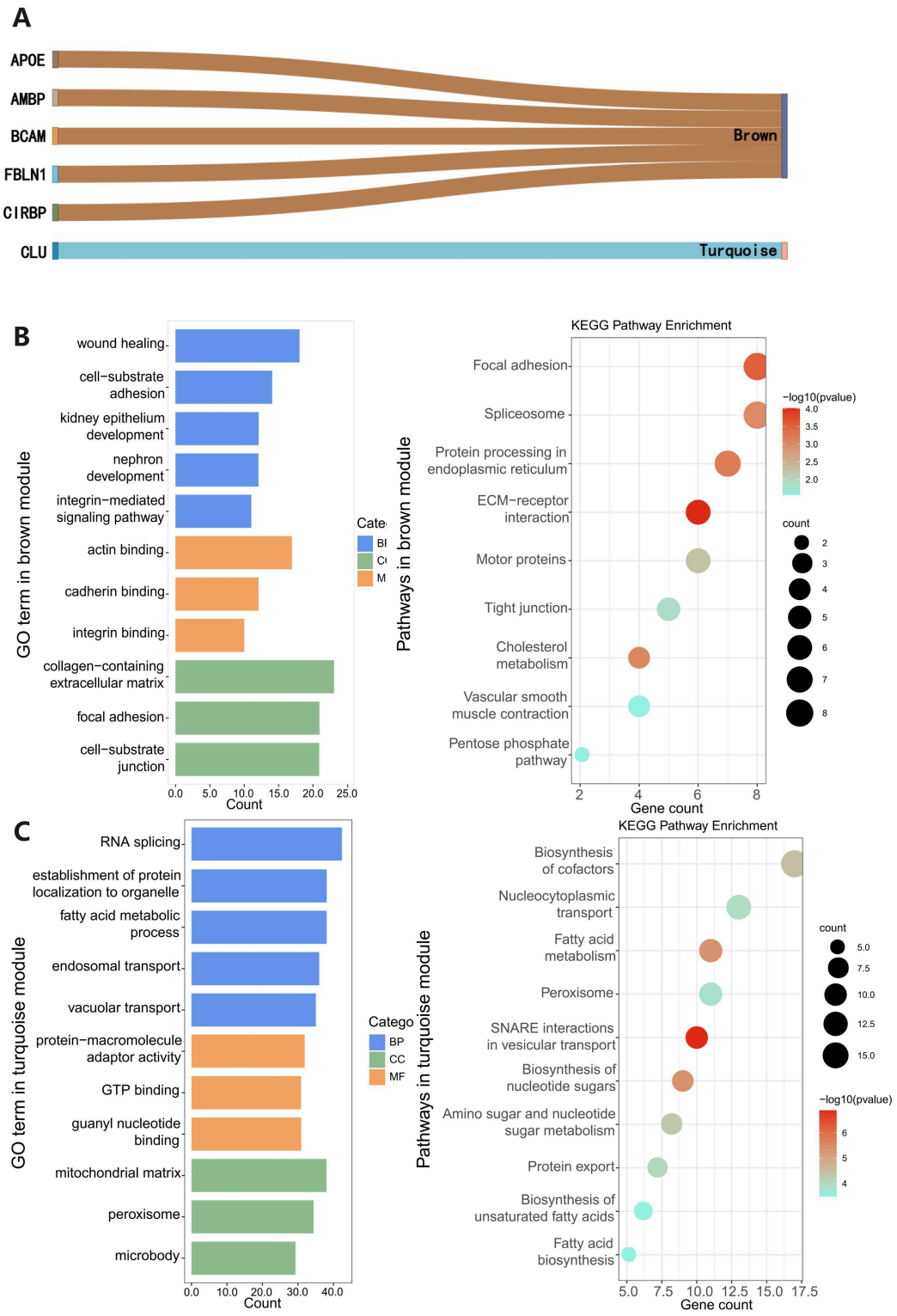


Figure 8

Hub protein distribution and functional enrichment of brown and turquoise WGCNA modules(A) Sankey plot mapping hub proteins to brown and turquoise modules. (B-C) GO and KEGG enrichment analyses for brown and turquoise modules separately.

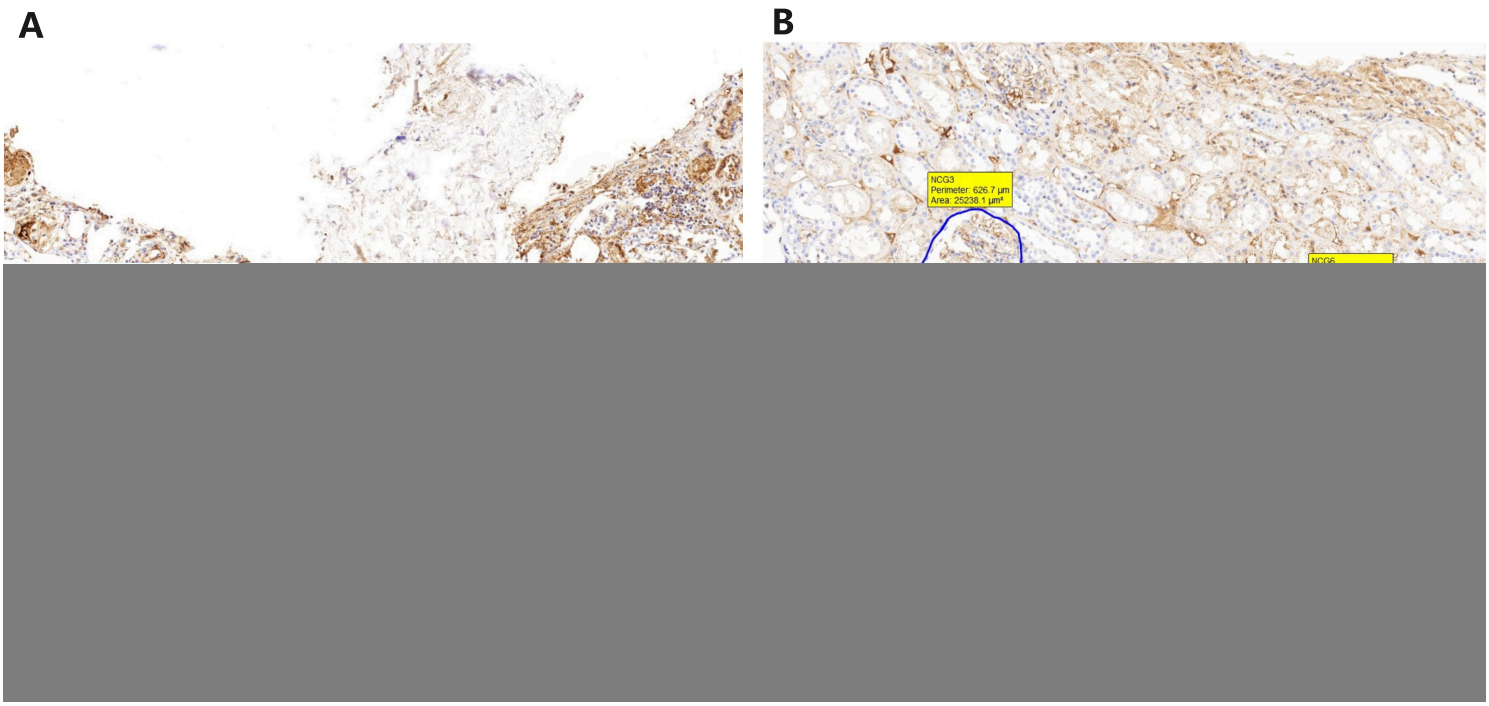


Figure 9

Immunohistochemistry comparison of glomerular target protein expression between MN and NC groupsLeft panel (A): MN group glomeruli; Right panel (B): NC group glomeruli. brown staining intensity reflects target protein abundance.

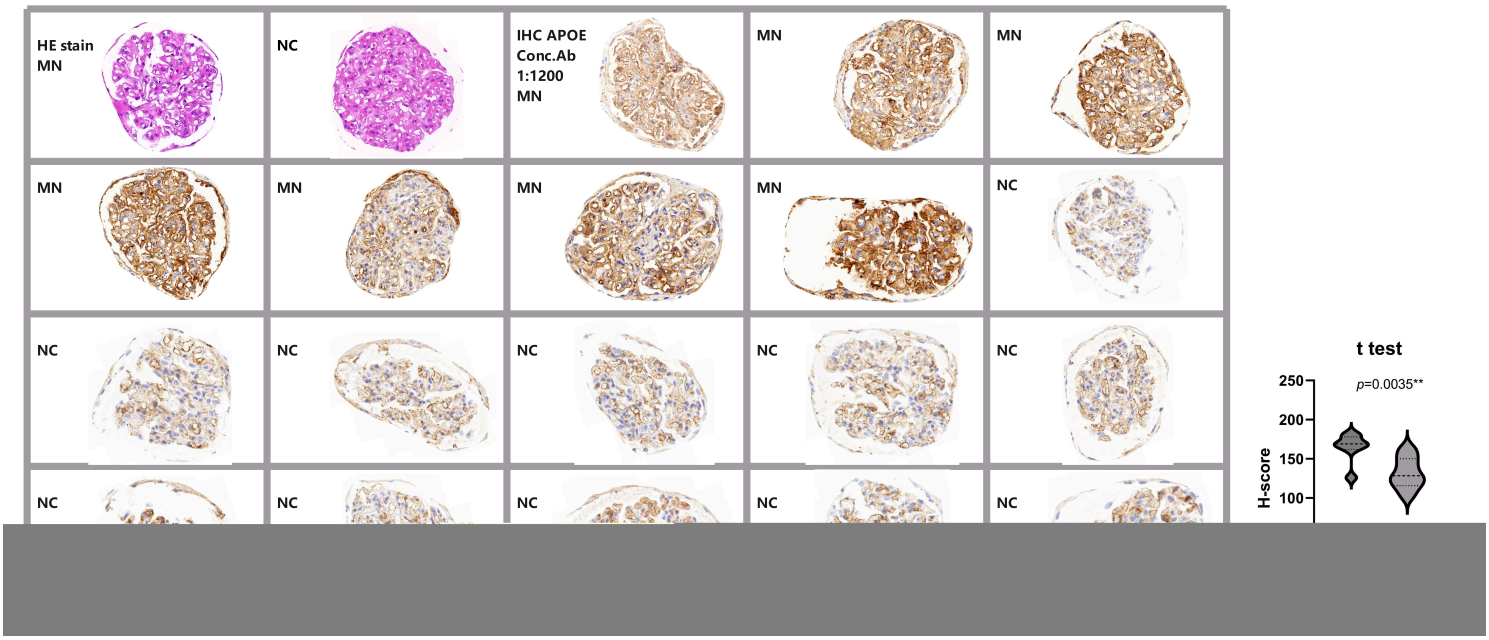


Figure 10

HE staining, APOE immunohistochemistry and H-score quantification of glomeruli from MN and NC cohortsTile view presents typical glomeruli histology and APOE IHC results; violin plot statistically

compares APOE H-scores, demonstrating significantly elevated glomerular APOE expression in MN patients (t-test, p=0.0035).

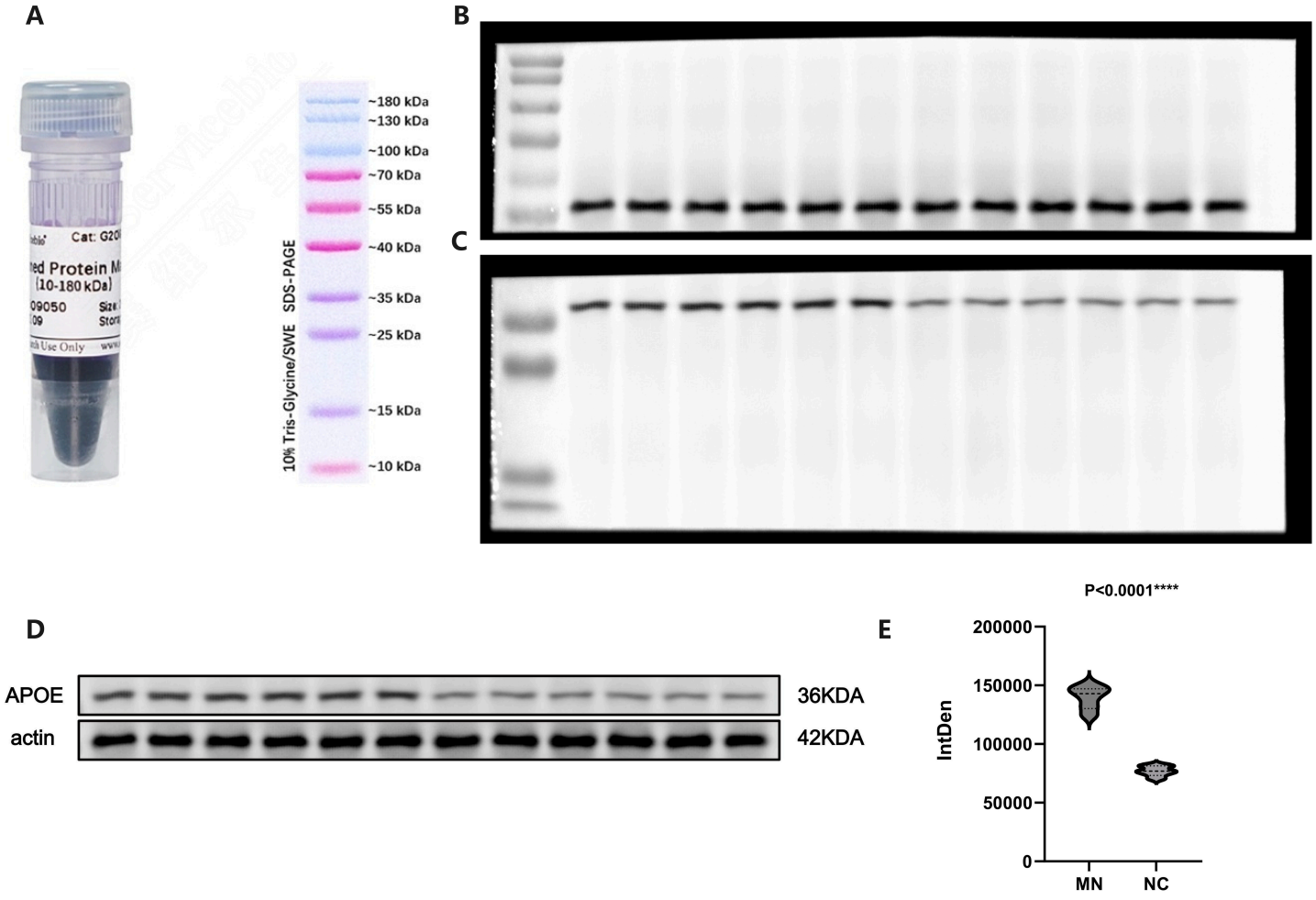


Figure 11

Western blot quantification of APOE expression(A) Prestained protein marker. (B-C) Uncropped blot images. (D) Cropped bands of APOE (36 kDa) and β-actin loading control (42 kDa). (E) Statistical comparison of band integrated density, showing significantly elevated APOE expression in MN group (P<0.0001).

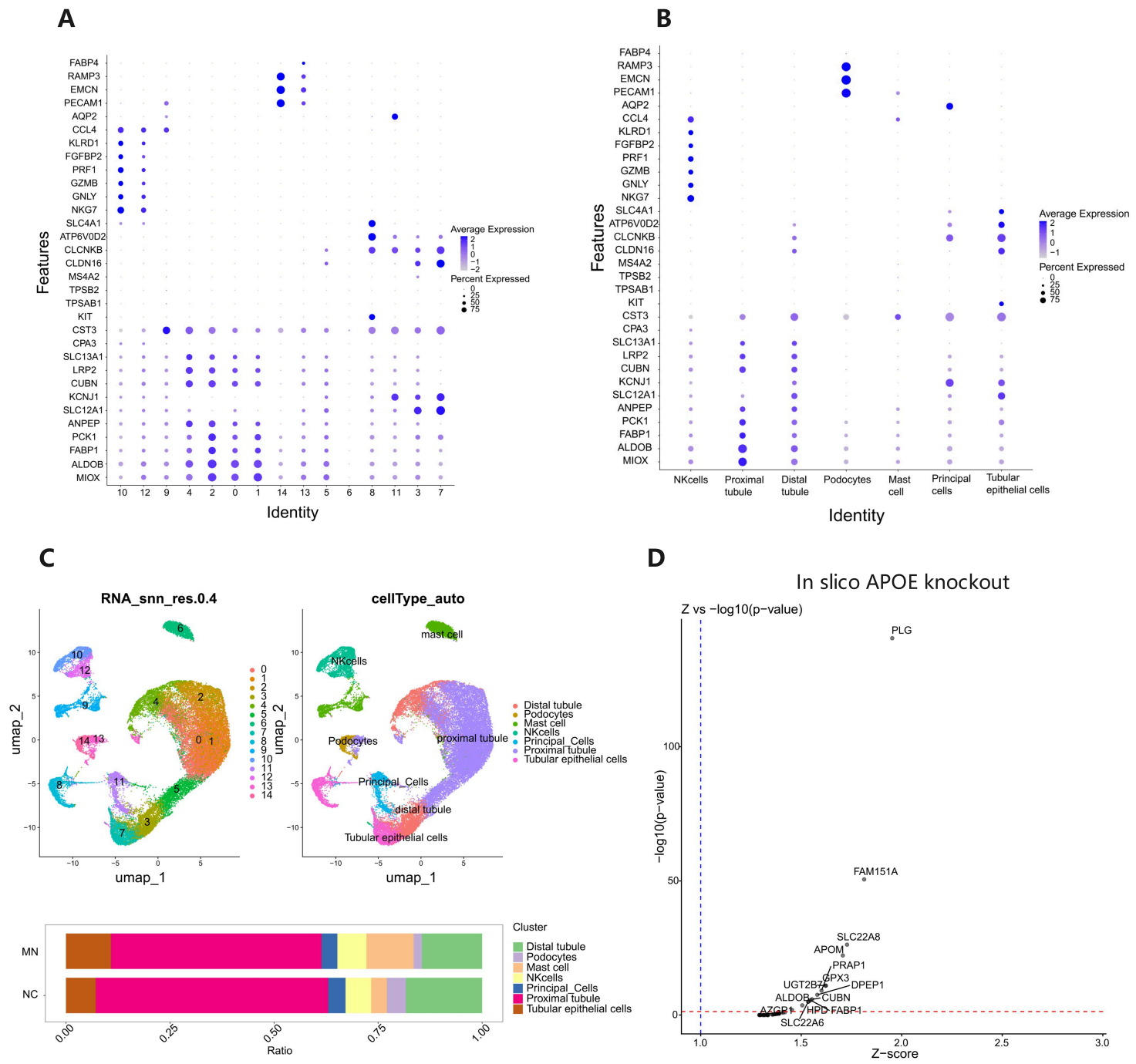


Figure 12

Single-cell annotation and APOE knockout simulation(A-B) Marker gene dot plots for unsupervised clusters and annotated renal cell populations. (C) UMAP clustering, cell type annotation and cell proportion comparison between MN and NC cohorts. (D) Volcano plot of differentially expressed genes from in silico APOE knockout.

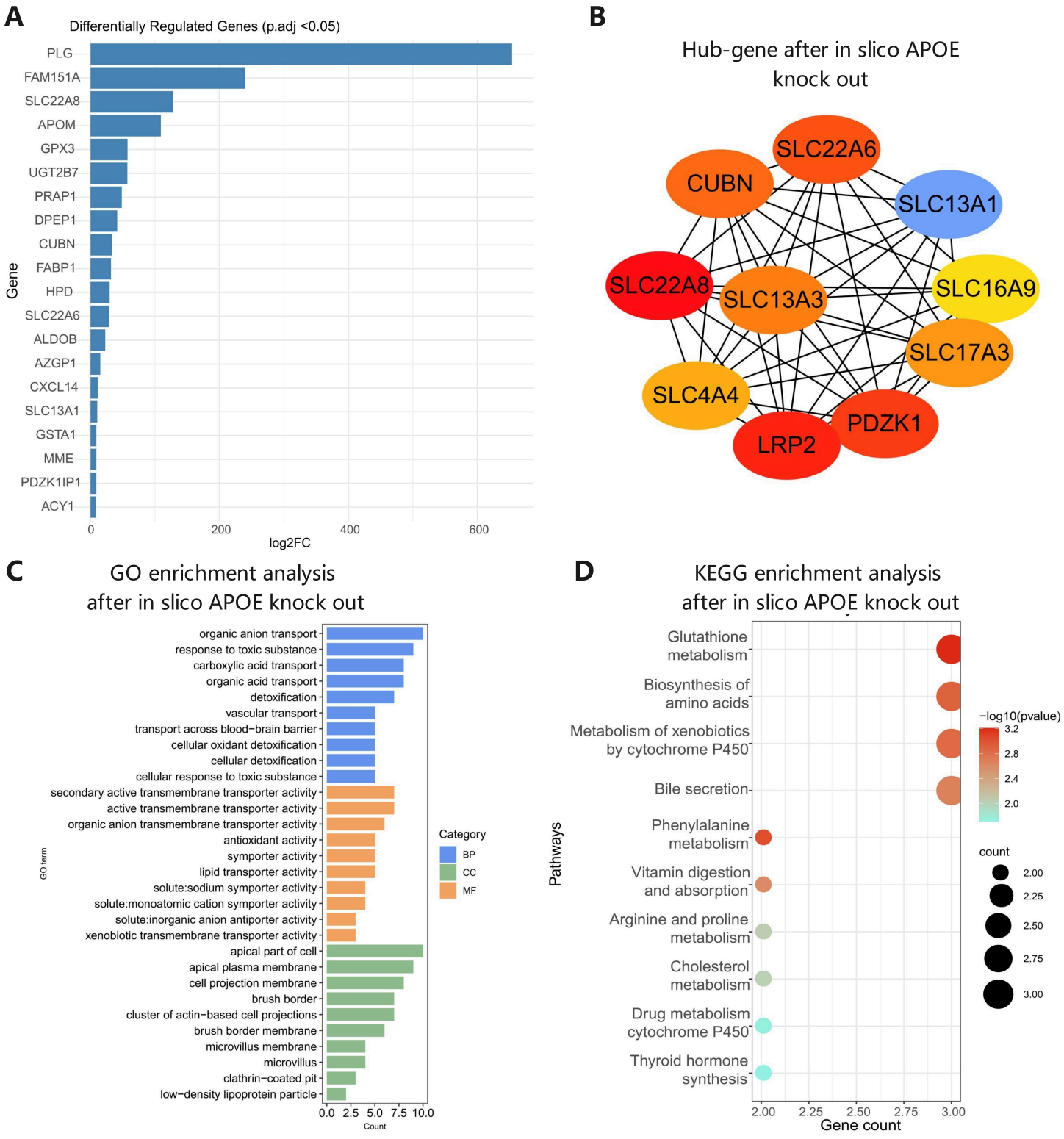


Figure 13

Bioinformatic analysis of transcriptomic changes upon in silico APOE knockout(A) Ranking of differentially expressed genes (adj.p<0.05) by log_2 fold change. (B) Hub gene interaction network constructed from differential genes. (C) GO enrichment results split across BP, CC and MF categories. (D) KEGG pathway enrichment showing enriched gene count and statistical significance via bubble attributes.

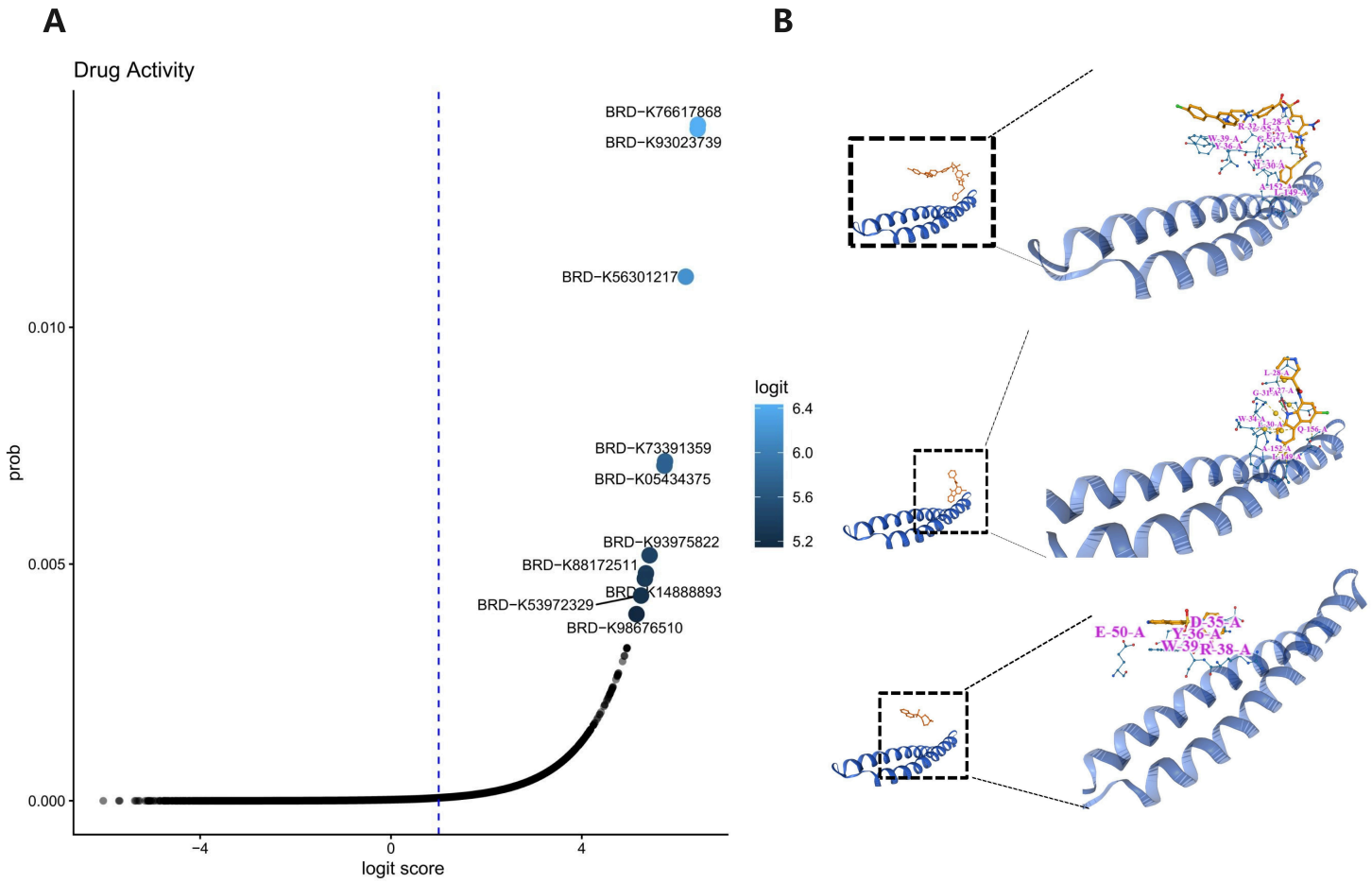


Figure 14

Drug screening and molecular docking analysis(A) Candidate compound screening based on logit score and predicted binding probability. (B) Docking poses of three screened small molecules binding to APOE, with critical interacting amino acid residues annotated in magnified views.

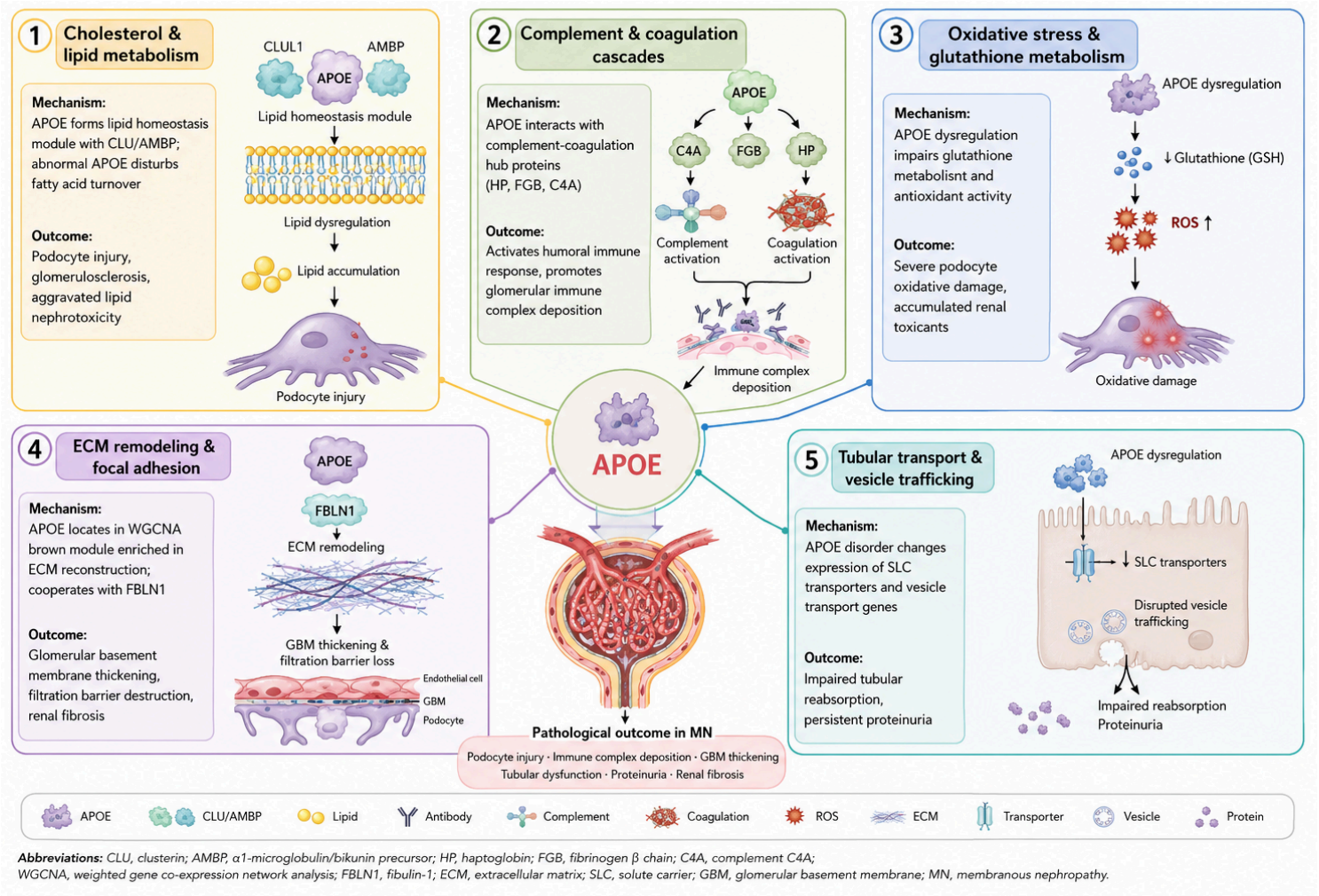


Figure 15

Working model: APOE drives MN pathogenesis through multiple pathological pathways

Five downstream pathological pathways modulated by APOE are illustrated: lipid metabolism disorder, complement-coagulation activation, oxidative stress, extracellular matrix remodeling, as well as impaired tubular vesicular transport. Synergistic effects of these pathways result in typical MN renal lesions including podocyte damage, filtration barrier defect and persistent proteinuria. Full abbreviations are listed at the bottom of the figure.

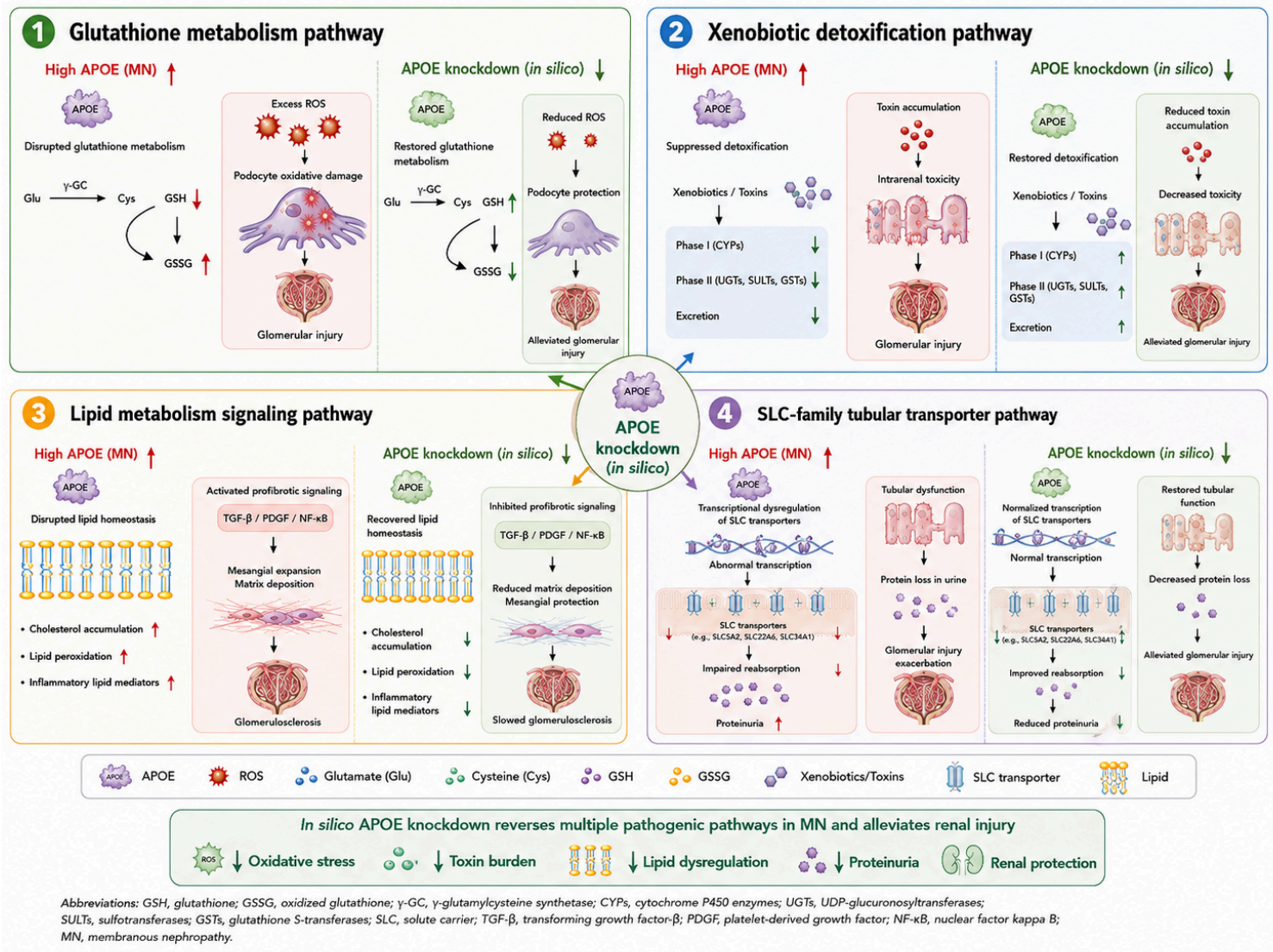


Figure 16

Four rescued pathways after in silico APOE knockdown in MN.Schematic illustrating how APOE knockdown restores glutathione metabolism, xenobiotic detoxification, lipid homeostasis and tubular SLC transporter function, countering major pathological features of MN and conferring renal protection. Full abbreviation definitions are listed below the schematic.

Supplementary Files

This is a list of supplementary files associated with this preprint. Click to download.

- gelbolt.tif
- actin.tif
- gel.jpg
- Table1.docx
- Table2.docx